DEVELOPMENTAL NEUROSCIENCE

Functional properties of habenular neurons are determined by developmental stage and sequential neurogenesis

Stephanie Fore[1], Francisca Acuña-Hinrichsen[1], Kadir Aytac Mutlu[1], Ewelina Magdalena Bartoszek[1], Bram Serneels[1], Nicholas Guy Faturos[1], Khac Thanh Phong Chau[1], Mehmet Ilyas Cosacak[2], Carmen Diaz Verdugo[1], Fabrizio Palumbo[1], Christa Ringers[1], Nathalie Jurisch-Yaksi[1,3,4], Caghan Kizil[2,5], Emre Yaksi[1]*

The developing brain undergoes drastic alterations. Here, we investigated developmental changes in the habenula, a brain region that mediates behavioral flexibility during learning, social interactions, and aversive experiences. We showed that developing habenular circuits exhibit multiple alterations that lead to an increase in the structural and functional diversity of cell types, inputs, and functional modules. As the habenula develops, it sequentially transforms into a multisensory brain region that can process visual, olfactory, mechanosensory, and aversive stimuli. Moreover, we observed that the habenular neurons display spatiotemporally structured spontaneous activity that shows prominent alterations and refinement with age. These alterations in habenular activity are accompanied by sequential neurogenesis and the integration of distinct neural clusters across development. Last, we revealed that habenular neurons with distinct functional properties are born sequentially at distinct developmental time windows. Our results highlight a strong link between the functional properties of habenular neurons and their precise birthdate.

INTRODUCTION

During development and maturation, the functional capacity of brain circuits increases to support the animals' expanding behavioral repertoire. For example, while a young zebrafish larva mostly needs to avoid threats and find food, more cognitively demanding behaviors such as associative learning (*1*, *2*) or social interactions (*3*) emerge later in development during the juvenile stage around 3 to 4 weeks. Such an expansion of the behavioral repertoire is a feature that is conserved across vertebrates (*4*) and is often accompanied with the development, establishment, and maturation of distinct circuit components generating functional modules within the brain (*5*). Hence, brain development and maturation is not only a linear expansion of the already existing building blocks but also a sequential increase in the diversity of functional modules and cell types. In the cortex, for example, individual layers are born at different time points, with deep layers being born earlier than superficial layers (*6*), creating a diversity in the cytoarchitecture of cortical layers and regions with distinct functions (*5*, *7*). Similarly, this chronological order of neurogenesis in larval zebrafish hindbrain and spinal cord was shown to generate functional diversity of neurons, which underlies increased sophistication of behaviors across development (*8*–*10*).

The maturation and refinement of the developing brain rely on neural activity that can be evoked by sensory inputs (*11*, *12*) or spontaneously generated (*11*, *13*). In most sensory systems, sensory-evoked activity was shown to be critical for the maturation of neural circuits and the refinement of topographical maps (*12*, *14*). The appearance of spontaneous activity of the developing brain starts early and coincides with periods of intense synaptogenesis and neuronal growth (*15*). For example, spontaneous activity bursts were observed in the visual, auditory, and somatosensory systems and are shown to be important for the remodeling of these structures (*13*, *14*). In higher brain regions, such as the hippocampus, large and slow bursts are observed (*16*) before the appearance of faster rhythms and the patterned activity of the adult hippocampus associated with learning and memory. Furthermore, spontaneous activity is also involved in the maturation of connections across distant brain regions, as observed between the olfactory bulb and the entorhinal cortex (*17*). Last, the synchronous bursting during spontaneous activity that is important in establishing neural connectivity was shown to be mediated via excitatory connections (*18*), gap junctions (*19*), glial cells (*20*), or other support cells (*21*). Together, both sensory-driven and spontaneous neural activity are essential in the development and maturation of neural circuits. It is, however, less clear how sensory-evoked and spontaneous neural activity interact as the animals develop.

While the majority of studies have focused on the development of sensory and motor systems, less is known about the maturation of higher brain areas integrating information from multiple brain regions, such as the habenula. The habenula is a particularly interesting brain region, as it was shown to integrate both sensory (*22*, *23*) and corticolimbic inputs (*24*–*26*) while directly regulating the function of monoaminergic brain nuclei controlling behavior (*23*, *25*, *27*). Dysfunction of the habenula is also shown to be associated with several neurological conditions and mood disorders including depression (*28*). The habenula is composed of several subdomains or modules based on its neurochemical profiles (*29*, *30*), anatomical projections (*31*–*33*), and the activity of habenular neurons (*33*–*35*).

[1]Kavli Institute for Systems Neuroscience and Centre for Neural Computation, Faculty of Medicine and Health Sciences, Norwegian University of Science and Technology, Olav Kyrres gata 9, 7030 Trondheim, Norway. [2]German Center for Neurodegenerative Diseases (DZNE) Dresden, Helmholtz Association, Tatzberg 41, 01307 Dresden, Germany. [3]Department of Clinical and Molecular Medicine, Norwegian University of Science and Technology, Olav Kyrres Gate 9, 7030 Trondheim, Norway. [4]Department of Neurology and Clinical Neurophysiology, St Olav University Hospital, Edvard Griegs Gate 8, 7030 Trondheim, Norway. [5]Center for Molecular and Cellular Bioengineering (CMCB), TU Dresden, Fetscherstr. 105, 01307 Dresden, Germany.
*Corresponding author. Email: emre.yaksi@ntnu.no

Two major subnuclei, the lateral and medial habenula in mammals, respectively, and the dorsal habenula (dHb) and ventral habenula (vHb) in zebrafish, have clear differences in their functional and molecular profiles (*33*). While the dHb is involved in sensory processing (*23*, *34*, *35*), aggression (*36*), and experience-dependent fear response (*27*, *31*), the vHb was shown to play a role in avoidance learning (*33*) and active coping behavior (*37*). In zebrafish, dHb and vHb originate from separate neural progenitor pools and were suggested to maturate at distinct developmental time points (*32*). Moreover, the dHb was shown to undergo asymmetric neurogenesis during the early stages of development, with left dHb neurons being born earlier than the ones in the right hemisphere (*38*). The prominent asymmetry in the molecular (*29*) and anatomical properties of habenula (*39*) is also reflected in its asymmetric encoding of visual and olfactory information in the left and the right dHb hemispheres, respectively (*34*, *35*). Recent transcriptome analysis further revealed multiple molecularly distinct and spatially organized functional modules within the zebrafish (*30*) and mammalian (*40*) habenula, which resemble the spatially organized functional clusters of habenular neurons during spontaneous activity (*35*). All of these evidences suggest a fine spatial organization of distinct functional modules within habenula (*35*). In addition, spontaneous habenular activity was shown to govern sensory responses and, therefore, proposed to represent internal states of the network, which could mediate the selection of appropriate behaviors (*35*). A recent study revealed a sequential recruitment of neurons generating an increase in vHb activity, during the switch from active to passive coping behaviors in juvenile zebrafish (*37*). Such complex behaviors emerge at later stages of zebrafish development (*1*, *3*), suggesting pronounced changes in the underlying circuitry across the brain. Despite extensive characterization of habenular circuitry during very early developmental stages (*29*, *38*, *39*), it is still unclear how the maturation of habenular networks during development corresponds to the establishment of its distinct functional modules.

In this study, we investigated how the function and the architecture of habenular networks change across development and how these alterations relate to the formation of distinct functional modules within habenula. We showed that as the habenula expands, the number of neurons increases, inhibitory connections are formed, and sensory inputs are integrated with a temporal order. Moreover, we revealed that the habenula is a multisensory brain region, which distinctly encodes different sensory modalities. Visual and olfactory responses in habenula develop early, while the responses to mechanosensory and aversive stimuli develop at later stages. Spontaneous habenular activity is present already at early developmental stages, and it is predictive of the habenular neurons with sensory responses. We observed a prominent restructuring of both spatial and temporal features of spontaneous habenular activity during development. These functional changes in the habenula were accompanied by a sequential and spatially organized addition of newly born neurons across development. Last, we showed that habenular neurons born at a distinct developmental stage exhibit similar functional properties. Our observations support the idea that neuronal birthdate and function are strongly related.

RESULTS

New neurons and new inhibitory connections are added to habenula during development

To study the functional development of zebrafish habenula, we focused on three developmental stages: early larval stage [3 days post-fertilization (dpf)], late larval stage (6 dpf), and juvenile stage (21 dpf). During these periods, zebrafish transition from self-feeding larvae (via the yolk sac) to an external feeding juvenile animal with more complex behaviors including those involving habenular circuits (*1*, *3*, *31*, *33*, *37*). First, we visualized the gross morphology of habenula in *Tg(elavl3:GCaMP6s)* (*41*) zebrafish, labeling most habenular neurons. We observed that the number of habenular neurons increases drastically from 3 to 21 days of zebrafish development (Fig. 1, A and B). Next, we investigated the expression of glutamate and γ-aminobutyric acid (GABA) by using *Tg(vglut2a:dsRed)* (*22*) and *Tg(gad1b:GFP)* (*42*) zebrafish. We found that at 3 dpf, habenula mainly consists of glutamatergic neurons, and as the animal gets older, few GABAergic neurons are added (Fig. 1C). From 6 dpf, we also observed prominent bilateral GABAergic projections that innervate specific domains at the lateral sides of habenula (Fig. 1C). These results suggest that habenula undergoes a nonlinear expansion with the addition of new cell types and inputs arriving at different time points throughout development.

Sensory inputs and computations in habenula follow a developmental order

Previous studies showed that habenula receives olfactory (*22*) and visual (*23*) inputs and responds to both of these sensory modalities (*34*, *35*, *43*). To investigate how these sensory inputs maturate during habenula development, we visualized the mitral cell and thalamic axon terminals in habenula using *Tg(lhx2a:gap-YFP)* (*22*) and *Et(−0.6hsp70l:Gal4-VP16) s1020t*; *Tg(UAS:nfsB-mCherry)* (*31*, *44*) zebrafish lines, respectively. At all ages, thalamic projections were found to innervate habenula (Fig. 2A, blue) in distinct locations that are different from GABAergic innervations (Fig. 2A, white) or mitral cell terminals (Fig. 2A, red). Yet, the density of olfactory bulb projections increased with age (Fig. 2A, red). These findings suggest that habenular neurons may be predominantly light responsive at younger ages, while odor responses develop later. To test this hypothesis, we measured odor (food odor) and light (red light flash) responses in the habenula by using two-photon calcium imaging in *Tg(elavl3:GCaMP6s)* (*41*) zebrafish. At 3 dpf, we found that a significantly higher portion of habenular neurons responds to the visual stimulus compared to food odor (Fig. 2, B and C). As zebrafish develop, the ratio of odor- and light-responding neurons became similar (Fig. 2, B and C). At all developmental stages, correlations between visual and olfactory stimuli were relatively low (Fig. 2D).

To further test whether the development of sensory responses in habenula is biased toward aversive or attractive stimuli within one sensory modality, we applied amino acid odor, food odor, skin extract, and ammonia, which were previously shown to elicit responses in the zebrafish habenula (*35*). Moreover, earlier studies revealed that amino acid odor (*45*) and food odor (*46*) elicit attraction, and skin extract (*47*) and ammonia (*46*) elicit freezing and defensive behaviors. While we did not observe any preference for habenular neurons to respond to aversive or attractive odors in 3-dpf zebrafish larvae, we observed that stimulation with aversive odors resulted in a higher number of responding neurons compared to attractive odors, in four out of four 21-dpf zebrafish (fig. S1, A and B). The correlations between aversive versus attractive odors were low in 3 dpf and increased at 21 dpf (fig. S1, C and D).

Previous studies showed that the zebrafish habenula can encode a diverse range of aversive experiences (*27*, *30*, *37*). To test the developmental order of zebrafish habenula for encoding aversive

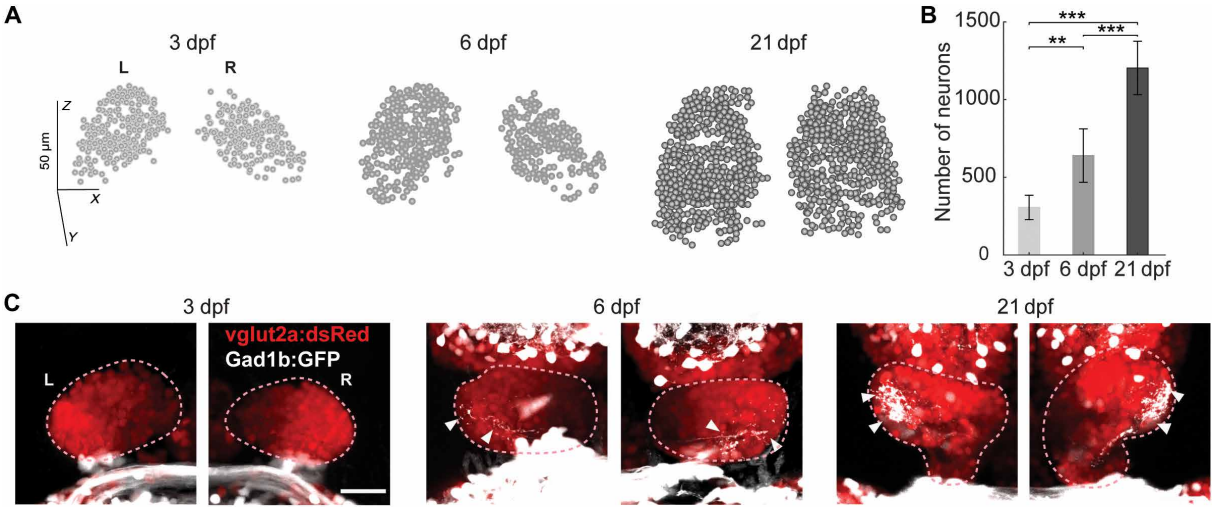

Fig. 1. During development, the number of habenular neurons increases and new GABAergic connections are added. (**A**) Representative examples of three-dimensional reconstructions of habenular neurons detected in *Tg(elavl3:GCaMP6s)* zebrafish line, using volumetric two-photon calcium imaging at three different developmental ages (3, 6, and 21 dpf). Coronal view. (**B**) The average number of neurons detected in *Tg(elavl3:GCaMP6s)* at 3 dpf ($n = 9$ fish), 6 dpf ($n = 6$ fish), and 21 dpf ($n = 9$ fish). $^{**}P < 0.01$ and $^{***}P < 0.001$, *t* test. Data are presented as means ± SEM. (**C**) Confocal microscopy projections of habenula in *Tg(vglut2a:dsRed)* and *Tg(gad1b:GFP)* double transgenic zebrafish at 3, 6, and 21 dpf, labeling glutamatergic (red) and GABAergic (white) neurons and projections, dorsal view. White arrowheads indicate GABAergic projections. Scale bar, 100 µm. L, left hemisphere; R, right hemisphere.

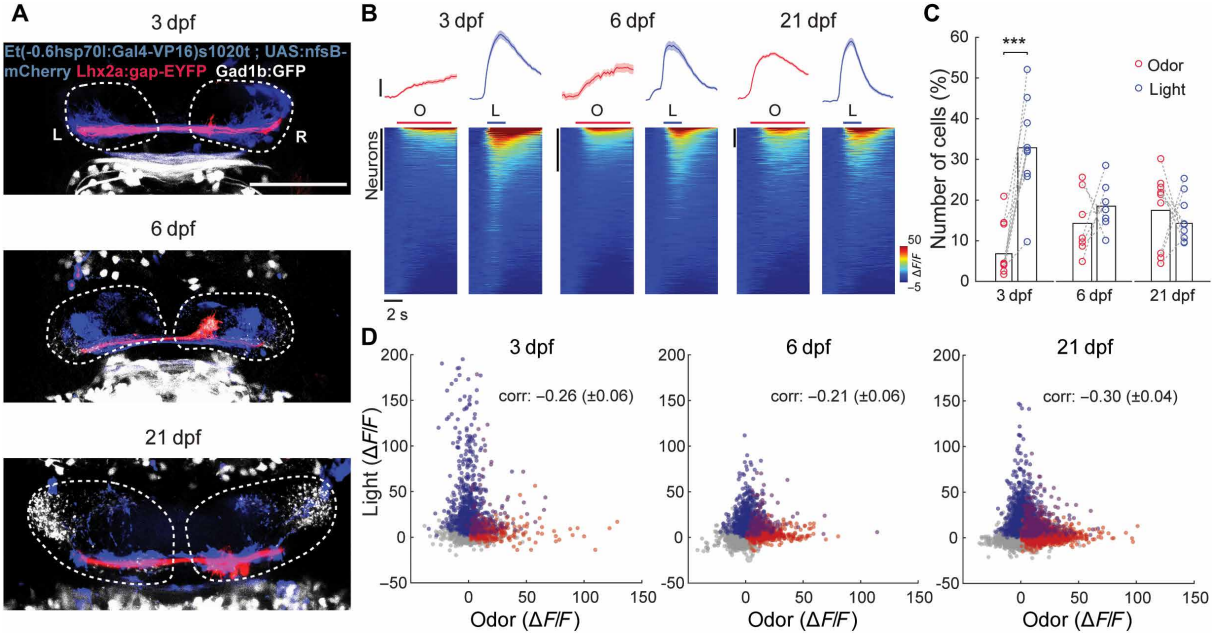

Fig. 2. Visual responses dominate larval habenula, while olfactory responses develop later. (**A**) Confocal microscopy projections of habenula in *Tg(Lhx2:gap-YFP)*; *Et(0.6hsp70l:Gal4-VP16) s1020t*; *Tg(UAS:nfsB-mCherry)* and *Tg(gad1b:GFP)* triple transgenic zebrafish labeling olfactory bulb projections (red), thalamic projections (blue), and GABAergic projections (white), dorsal view. Dashed white lines delineate habenula. Scale bar, 100 µm. L, left hemisphere; R, right hemisphere. (**B**) Top panel shows average responses of odor-responding (red) and light-responding habenular neurons (blue) over four to five trials at 3 dpf ($n = 9$), 6 dpf ($n = 7$), and 21 dpf ($n = 9$) zebrafish. Black bars represent 10% Δ*F*/*F*. Shadows represent SEM. Bottom panel shows color-coded sensory responses (Δ*F*/*F*) of all individual Hb neurons exposed to 5-s odor (O; red) stimulus (left) and 2-s light (L; blue) stimulus (right) in all fish imaged at 3, 6, and 21 dpf. Black bars represent 1000 neurons. (**C**) Percentage of odor (red dots) versus light (blue dots) responding neurons at 3, 6, and 21 dpf. $^{***}P < 0.001$, paired *t* test. All data are presented as means ± SEM. (**D**) Odor (red) versus light (blue) response amplitude of all habenular neurons responses at 3, 6, and 21 dpf. Magenta color depicts the neurons responding to both odor and light. Gray dots represent nonresponsive neurons. Average ± SEM correlations between different stimulus representations by habenular responses are represented by "corr." Note that at all ages, odor and light responses are dissimilar, depicted by the negative correlations.

stimuli, we applied mechanical vibrations (*48*) and mild electric stimulation (*27*, *30*, *37*), both of which were shown to generate aversive reactions in developing zebrafish (*27*, *30*, *37*, *48*). We also compared these aversive stimuli to visual responses in the habenula evoked by red light. Consistent with our results above (Fig. 2), the zebrafish habenula predominantly responds to visual stimulation at 3 dpf (Fig. 3, A and B). As zebrafish develop, we observed that a significantly larger number of habenular neurons responded to mild electric stimulation at 6 and 21 dpf (Fig. 3B). Moreover, we observed that significantly larger number of habenular neurons respond to light compared to mechanical vibrations at 6 dpf (Fig. 3B). At 21 dpf, we no longer observed any significant difference between the number of neurons responding to light, electric stimuli, and vibrations (Fig. 3B). These three different stimulus modalities exhibit low correlations at all developmental stages (Fig. 3C). All these results suggest that while the 3-dpf habenula preferentially responds to light, the animal develops significantly more habenular neurons respond to aversive electrical stimuli, as the animal develops. Together, the developing habenula can selectively encode an expanding number of sensory modalities with an increasing preference for aversive electrical stimuli at later stages.

Functional lateralization of visual and olfactory responses decreases across development, and it is not prominent for aversive stimuli

Earlier studies revealed a strong molecular (*29*, *32*) and functional (*34*) lateralization of habenular networks, especially across the dHb hemispheres of larval zebrafish. There is no evidence for such lateralization in the rodent habenula, which is mostly studied in adults by using aversive stimuli (*25*, *26*). This made us question whether the ontogeny of functional lateralization in the zebrafish habenula might resemble the phylogeny of the vertebrate habenula, where lateralized responses to light and odors appear first and non-lateralized responses to aversive stimuli develop later. To test this hypothesis, we investigated the lateralization of sensory responses in habenular neurons across zebrafish development. First, we showed that the dorsal sections of habenula, which likely cover the dHb, exhibit lateralized visual and olfactory responses at all ages (Fig. 4, A and B). We quantified this functional lateralization by measuring the ratio of light- versus odor-responding habenular neurons across hemispheres (*34*) and by using a lateralization index, where 0 represents symmetry and 1 represents complete segregation of light and odor responses across hemispheres. Across development, dHb exhibits high functional lateralization of light and odor responses, when compared to the ventral sections of habenula (Fig. 4B). Yet, we also observed that the functional lateralization of habenular circuits significantly decreases across development (Fig. 4, C and D). Despite this decrease, light and odor responses exhibit prominent spatial organization (Fig. 4E), quantified by the focality index, ranging from 0 (for random spatial distribution of sensory responses) to 1 (for maximally focal sensory responses) (*49*). Instead, aversive stimuli elicited no such lateralization across habenular hemispheres (fig. S2), resembling the nonlateralized aversive cue representations in the rodent habenula (*25*, *26*). These results indicate that functional lateralization is a feature of dHb (*34*) that develops earlier and preferentially responds to visual and olfactory stimuli. Instead, vHb,

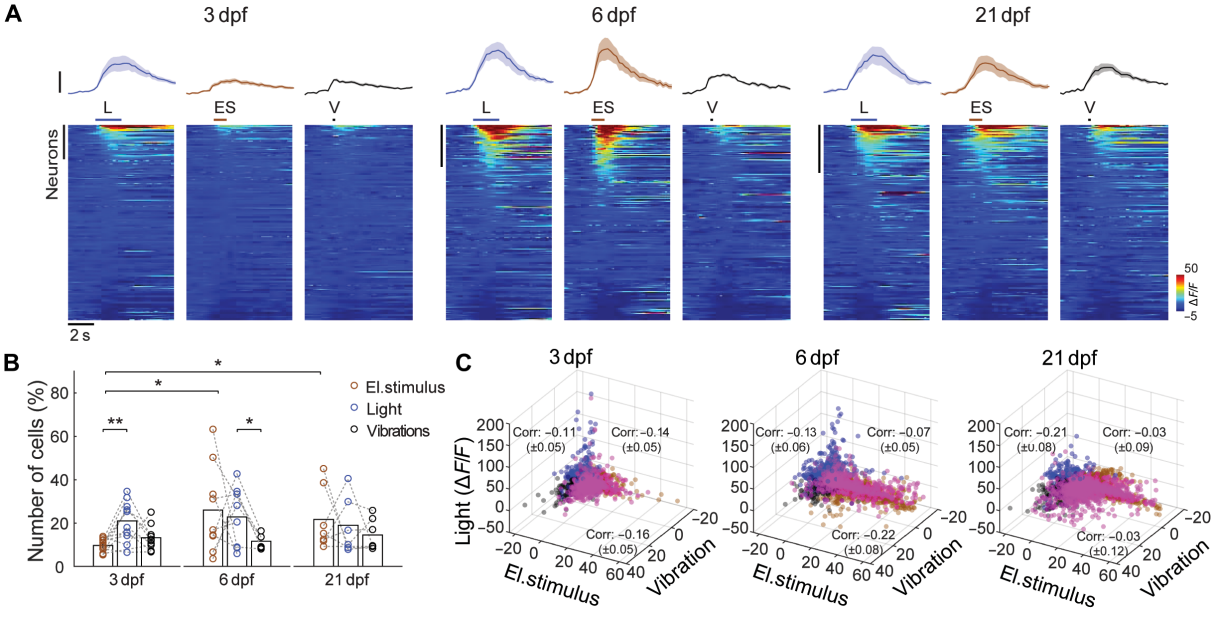

Fig. 3. Aversive electrical stimuli and mechanical vibrations are encoded in developing habenula. (**A**) Top panel shows average responses in habenular neurons to light (L; blue), mild electric stimulation (ES; brown), and mechanical vibrations (V; black) over four to five trials in 3 dpf ($n = 11$), 6 dpf ($n = 9$), and 21 dpf ($n = 7$) zebrafish. Black bars represent 10% $\Delta F/F$. Shadows represent SEM. Bottom panel shows color-coded sensory responses ($\Delta F/F$) of all individual Hb neurons exposed to 2-s light stimulus (left), 1-s mild electric stimulation (middle), and 0.05 s mechanical vibration (right) in all fish imaged at 3, 6, and 21 dpf. Black bars represent 1000 neurons. (**B**) Percentage of responding neurons to light (blue), mild electric stimulus (brown), and mechanical vibrations (black) at 3, 6, and 21 dpf. $^*P < 0.05$ and $^{**}P < 0.01$, paired *t* test for the comparisons within groups and unpaired *t* test for comparisons between groups. (**C**) Light (blue) versus mild electric stimulus (brown) versus mechanical vibrations (black) response amplitude of all habenular neuron responses at 3, 6, and 21 dpf. Magenta color depicts the neurons responding to more than one stimulus. Average ± SEM Pearson's correlation coefficients between different stimulus representations by habenular responses are represented by "corr." Note that at all ages, different stimulus modalities are distinctly represented, depicted by the negative correlations. All data are presented as means ± SEM.

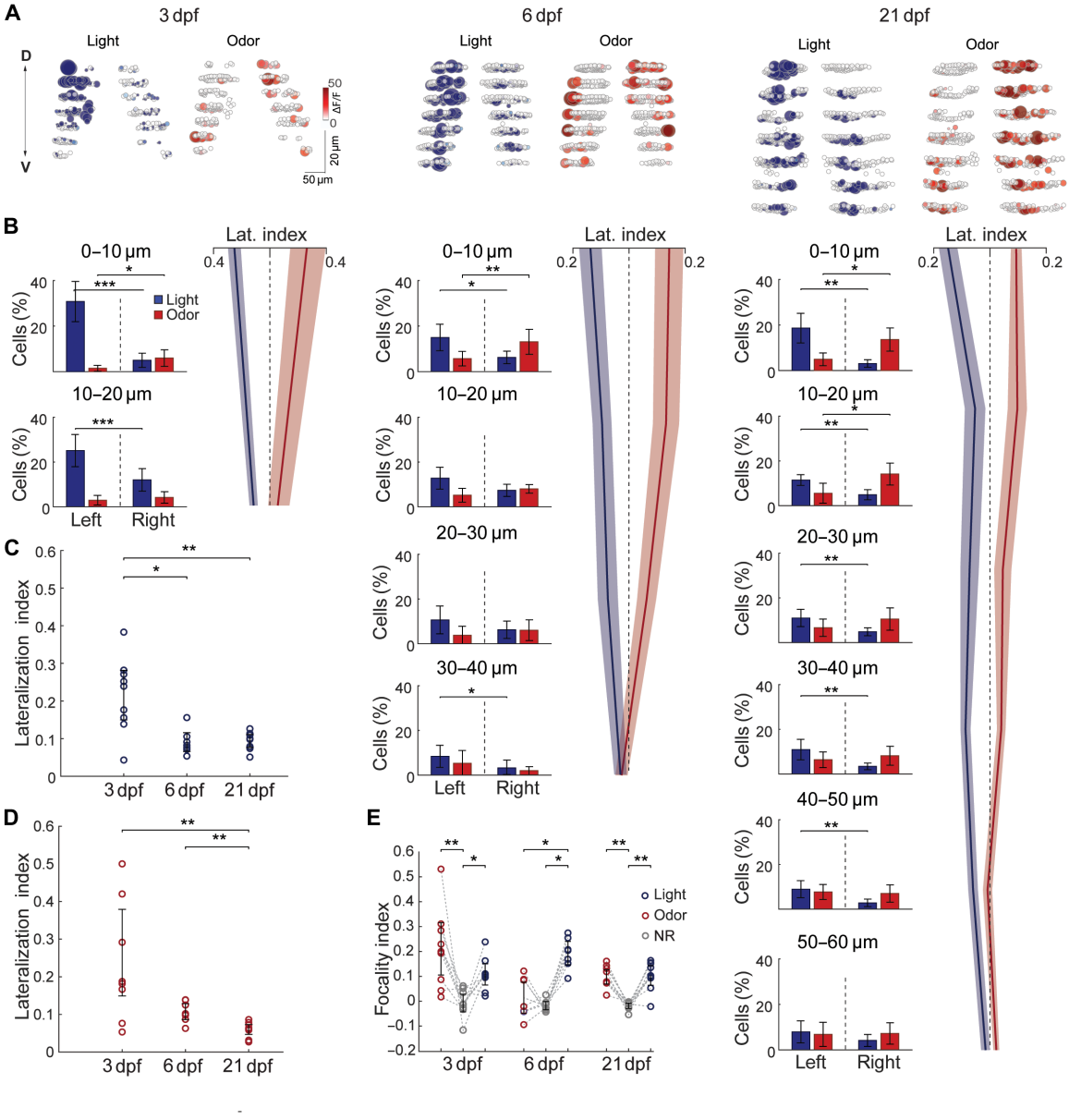

Fig. 4. Sensory lateralization is prominent in dHb at all ages but decreases with age especially in vHb. (**A**) Three-dimensional reconstructions of habenular responses to light (blue) and odor (red) stimulation recorded by volumetric two-photon microscopy in *Tg(elavl3:GCaMP6s)* zebrafish, at 3, 6, and 21 dpf. White dots indicate nonresponding neurons. Coronal view. (**B**) The ratio of odor (red) versus light (blue) responding neurons in left versus right habenular hemispheres, as well as associated sensory lateralization index at 3 dpf (left), 6 dpf (middle), and 21 dpf (right) zebrafish. Each row represents the average values for neurons within the 10-μm plane (from the top to bottom). Shades represent ±SEM; 3 dpf ($n = 9$ fish), 6 dpf ($n = 7$ fish), and 21 dpf ($n = 9$ fish). $^{*}P < 0.05$, $^{**}P < 0.01$, and $^{***}P < 0.001$, *t* test. (**C**) Average lateralization index of light responses for the entire habenula of all fish at 3, 6, and 21 dpf. $^{*}P < 0.05$ and $^{**}P < 0.01$, Wilcoxon rank sum test. (**D**) Average lateralization index of odor responses for the entire habenula of all fish at 3, 6, and 21 dpf. $^{**}P < 0.01$, Wilcoxon rank sum test. (**E**) Focality index for odor-responding (red) and light-responding (blue) neurons compared to NR (nonresponding neurons, gray) at 3, 6, and 21 dpf. $^{**}P < 0.01$ and $^{***}P < 0.001$, Wilcoxon signed-rank test. All data are presented as means ± SEM.

which develops later during development, does not exhibit prominent functional lateralization.

Functional clusters of habenular neurons exhibit spatially organized spontaneous activity at all ages

In juvenile zebrafish, spatially organized functional clusters of habenular neurons display synchronous bursts of spontaneous activity, which is present even in the absence of sensory inputs (*35*). It is, however, less clear if such spontaneous activity is also present in younger zebrafish larvae and to what extent it changes across habenular development. To study this, we recorded ongoing habenular activity in the absence of external stimuli at different developmental stages. We observed that clusters of habenular neurons exhibit correlated spontaneous activity already at 3 dpf (Fig. 5A). Next, we investigated the stability of these functional clusters during different time windows, using k-means clustering (*35*). We showed

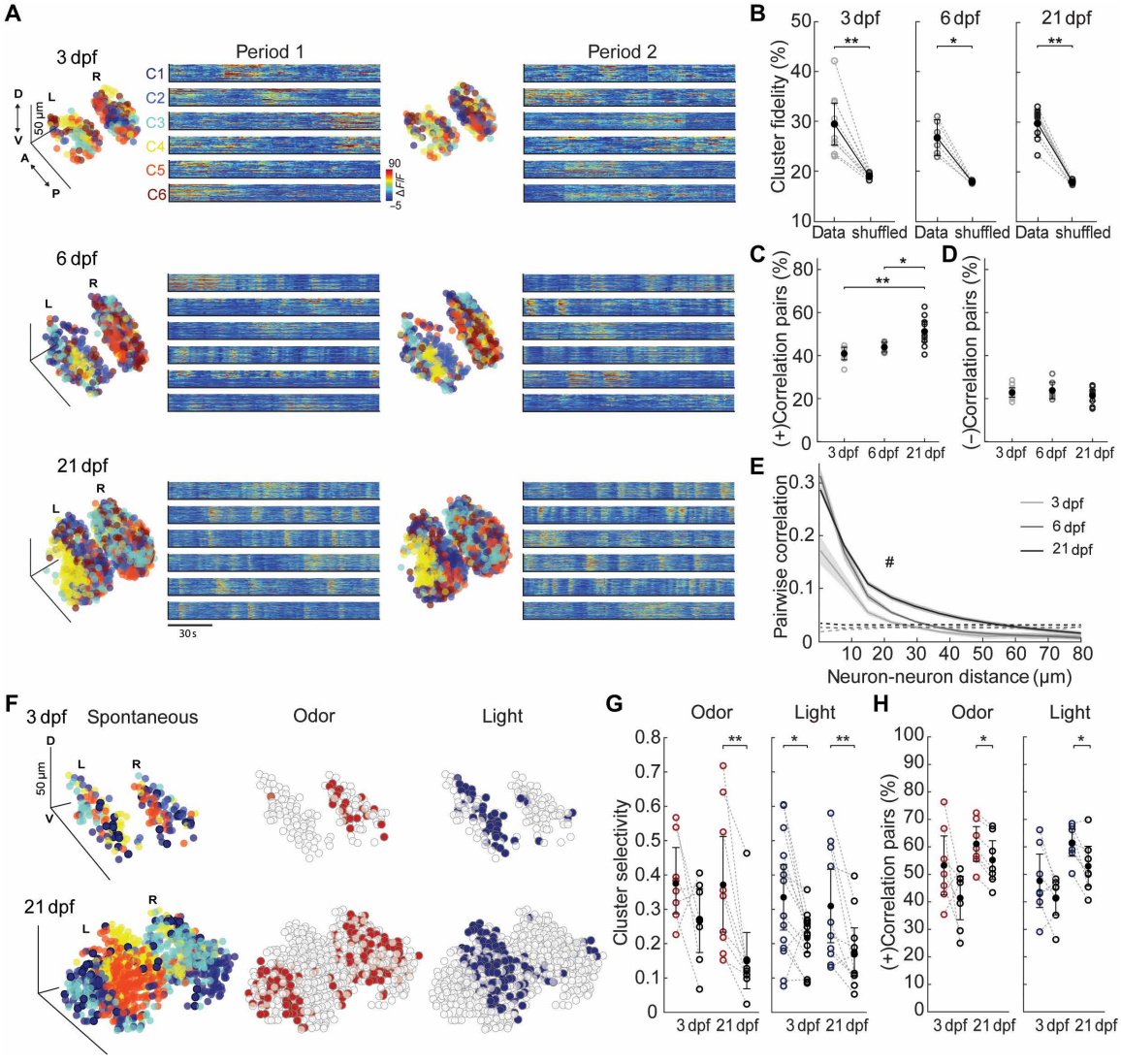

Fig. 5. Spontaneous habenular activity is structured into spatially organized functional clusters of neurons that are preserved during sensory responses, at all ages. (**A**) Functional clusters of habenular neurons with synchronous spontaneous activity in two different time periods (period 1 and period 2). Three-dimensional reconstruction depicts the spatial locations of all neurons. Each color represents a neuronal cluster with similar spontaneous activity, defined by using k-means clustering. Color-coded neural traces on the right show the spontaneous activity of each neuron that belongs to a given cluster "C." Warm color represents increased neural activity. Each row represents an example zebrafish at 3, 6, and 21 dpf. D, dorsal; V, ventral; A, anterior; P, posterior. (**B**) Cluster fidelity, depicting the ratio of neural pairs that remain within the same functional cluster during two different time periods for 3 dpf ($n = 9$), 6 dpf ($n = 6$), and 21 dpf ($n = 9$), compared to shuffled chance levels. *$P < 0.05$ and **$P < 0.01$, Wilcoxon signed-rank test. (**C**) The ratio of neural pairs with significant ($P < 0.05$) positive correlations during two periods of spontaneous activity. *$P < 0.05$ and **$P < 0.01$, Wilcoxon rank sum test. (**D**) The ratio of neural pairs with significant ($P < 0.05$) negative correlations during two periods of spontaneous activity. Wilcoxon rank sum test. (**E**) Relation between pairwise correlation of spontaneous neural activity and the distance between each neuron pair in habenula at 3, 6, and 21 dpf. Dashed lines represent the results when neuron locations are shuffled. ANOVA-n displayed significance over distances ($P < 0.001$) and over age groups ($P < 0.001$) indicated with #. (**F**) Color-coded functional clusters of habenular neurons with synchronous spontaneous activity for an example zebrafish at 3 (top) and 21 (bottom) dpf. On the middle and right panels, odor (red) and light (blue) responses of the same neurons are visualized. Scale bars, 50 µm. (**G**) Cluster selectivity, depicting how odor-responding (red) or light-responding (blue) neurons are distributed into functional clusters based on their spontaneous activity. High selectivity means that both odor- and light-responding neurons belong to fewer clusters compared to the same number of randomly selected nonsensory neurons (gray dots), at 3 and 21 dpf. (**H**) The ratio of neural pairs with significant ($P < 0.05$) positive correlations of spontaneous activity, for odor- and light-responsive neurons, when compared to the same number of randomly selected nonsensory neurons, at 3 and 21 dpf. *$P < 0.05$, **$P < 0.01$, Wilcoxon signed-rank test. All data are presented as means ± SEM.

that at all developmental stages, a large portion of habenular neurons that belong to a functional cluster remain in their respective cluster with a significantly higher probability compared to chance levels (Fig. 5B). To investigate the synchrony between the habenular neurons further, we next computed the ratio of significantly positive and negative correlated pairs of habenular neurons. We observed that as the animal develops, more pairs of neurons displayed significant and robust positive correlations (Fig. 5C). We did not observe such a change for negative correlations between habenular neurons (Fig. 5D). Next, we investigated the spatial organization of

synchronous habenular activity by plotting the average pairwise correlation of neurons versus the distance between them. We observed that while nearby habenular neurons have more correlated spontaneous activity at all developmental stages, they exhibit significantly stronger correlations during older developmental stages (Fig. 5E). This increase in the ratio (Fig. 5C) and strength (Fig. 5E) of positive correlations is likely due to the maturation of synaptic connections between habenular neurons, as well as the arrival of synaptic inputs to habenula.

Next, we investigated whether habenular neurons with correlated spontaneous activity also respond to sensory stimulation similarly and how this changes across development. We observed that, especially at later developmental stages, odor- and light-responsive habenular neurons largely overlap with the distinct functional clusters with correlated spontaneous activity, compared to the same number of randomly selected nonsensory neurons (Fig. 5, F and G). This was also true when comparing sensory responding neurons to all nonresponding neurons (fig. S3). Only in older zebrafish did we observe that odor- or light-responding habenular neurons exhibit a significantly higher ratio of positive correlations during spontaneous activity, compared to the same number of randomly selected nonsensory habenular neurons (Fig. 5H). These results highlight the developmental maturation of habenular circuits while generating more structured spontaneous activity that better predicts the sensory response characteristics of habenular neurons.

Features of spontaneous habenular activity change during development

Our results revealed that already at early developmental stages, the habenula exhibits prominent spontaneous activity. In several brain regions, spontaneous activity during early development is generally characterized as large bursts with long quiescent intervals (*16*), whereas adult brains usually exhibit rhythmic activity at faster frequencies (*16*, *50*). To test whether the temporal features of habenular activity are changing over development, we detected the spontaneous activity bursts (*51*) (Fig. 6A) and quantified the frequency and duration of these events. We observed that as the animals develop, the frequency of spontaneous activity bursts significantly increases (Fig. 6B) and their duration decreases (Fig. 6C). Moreover, while the average activity of habenular neurons decreases (Fig. 6D), a larger proportion of habenular neurons shows spontaneous activity (Fig. 6E) at later developmental stages. These results are in line with the developmental changes observed in other vertebrate brain regions and highlight the maturation of habenular spontaneous activity across development.

Next, we asked whether such temporal features (i.e., burst duration and frequency) of spontaneous habenular activity are also spatially organized. We quantified the spatial distribution by using the measure of focality index, ranging from 0 (for random spatial distribution) to 1 (for an extremely focal point) (*49*). At all developmental stages, the temporal features of habenular spontaneous activity, burst frequency, and duration were highly focal and not randomly distributed (Fig. 6F, also note the mean focality values). To further investigate the spatial distribution of habenular activity at different developmental stages, we adopted a commonly used reporter of neural activity, phospho-ERK (extracellular signal–regulated kinase)/total-ERK (pERK/tERK) ratio (*52*). We observed that during early developmental stages, pERK/tERK ratio is distributed rather uniformly across the habenula (Fig. 6, G and H, top), while at later developmental stages, pERK/tERK ratio was concentrated more laterally (Fig. 6, G and H, bottom), indicating a higher neural activity toward the lateral ends of habenula. We also observed that the most silent habenular neurons (black dots in Fig. 5F) were located closer to the medial wall of habenula (Fig. 6I), near the location of habenular neural progenitors labeled in *Tg(her4.1:GFP)* (*53*) zebrafish (Fig. 7A).

Since the juvenile zebrafish habenula displayed an increased pERK/tERK ratio toward the lateral ends (Fig. 6, G and H) and a higher number of silent neurons toward the medial ends (Fig. 6I), we hypothesized that the mediolateral distribution of habenular neurons at older stages might represent their physiological and developmental maturity. To test this hypothesis, we performed intracellular recordings of habenular neurons across the mediolateral axis of juvenile zebrafish at later developmental stages. We observed that the input resistance, a hallmark of developmental maturation of cortical neurons (*7*), was significantly higher for medial habenular neurons, compared to lateral habenular neurons (Fig. 6J). Together, this suggests that neurons near the lateral ends of habenula might be more mature neurons that are born during early developmental stages, compared to medial habenula neurons born later.

Distinct spatial domains of habenular neurons are born through sequential neurogenesis

Next, we asked whether the spatial organization of habenula across the mediolateral axis might be a result of sequential neurogenesis across development. To test this hypothesis, we first investigated the location of habenular neurogenesis. We observed that neural progenitors labeled by *Tg(her4.1:GFP)* (*53*) expression are located at the medial walls of habenular hemispheres (Fig. 7A). To further investigate the relationship between the birthdate of habenular neurons and their spatial distribution, we labeled habenular neurons born during different developmental stages using 5-bromo-2′-deoxyuridine (BrdU) incorporation (Fig. 7B). BrdU birthdating showed that the habenular neurons that are born during distinct developmental stages were spatially organized (Fig. 7C). Moreover, we observed that the birthdate of habenular neurons is a good indicator for their spatial location, where oldest neurons (born early in development) mostly occupied the lateral wall of habenula and youngest neurons (born late in development) were closest to the medial wall (Fig. 7, C and D).

Next, we developed an in vivo birthdating method to further investigate the distinct clusters of habenular neurons that are born during different developmental stages. To do this, we adopted a previously described approach to label cohorts of mammalian cortical neurons born at distinct developmental stages (*54*). We achieved this by injecting two different colors (far-red and green) of a fluorescent cell tracer in the telencephalic ventricle (*55*), near the neural progenitor zone on the medial wall of habenula (Fig. 7A) of 2.5- and 5-dpf zebrafish larvae (Fig. 7E). Fifteen hours after the cell tracer injections, only the cells near the medial wall of habenula were labeled (Fig. 7E). We raised the zebrafish larvae injected with cell tracers of two different colors (far-red and green) until 12 and 21 dpf and visualized the cohorts of birthdated habenular neurons in living juvenile zebrafish (Fig. 7F). Our results revealed a distinct spatial organization of habenular neurons birthdated at 2.5 dpf, compared to the neurons birthdated at 5 dpf (Fig. 7F). Furthermore, we observed less than 4% overlap of birthdated neurons by injections at 2.5 versus 5 dpf, highlighting the temporal resolution of our in vivo birthdating method (Fig. 7G). In addition, these

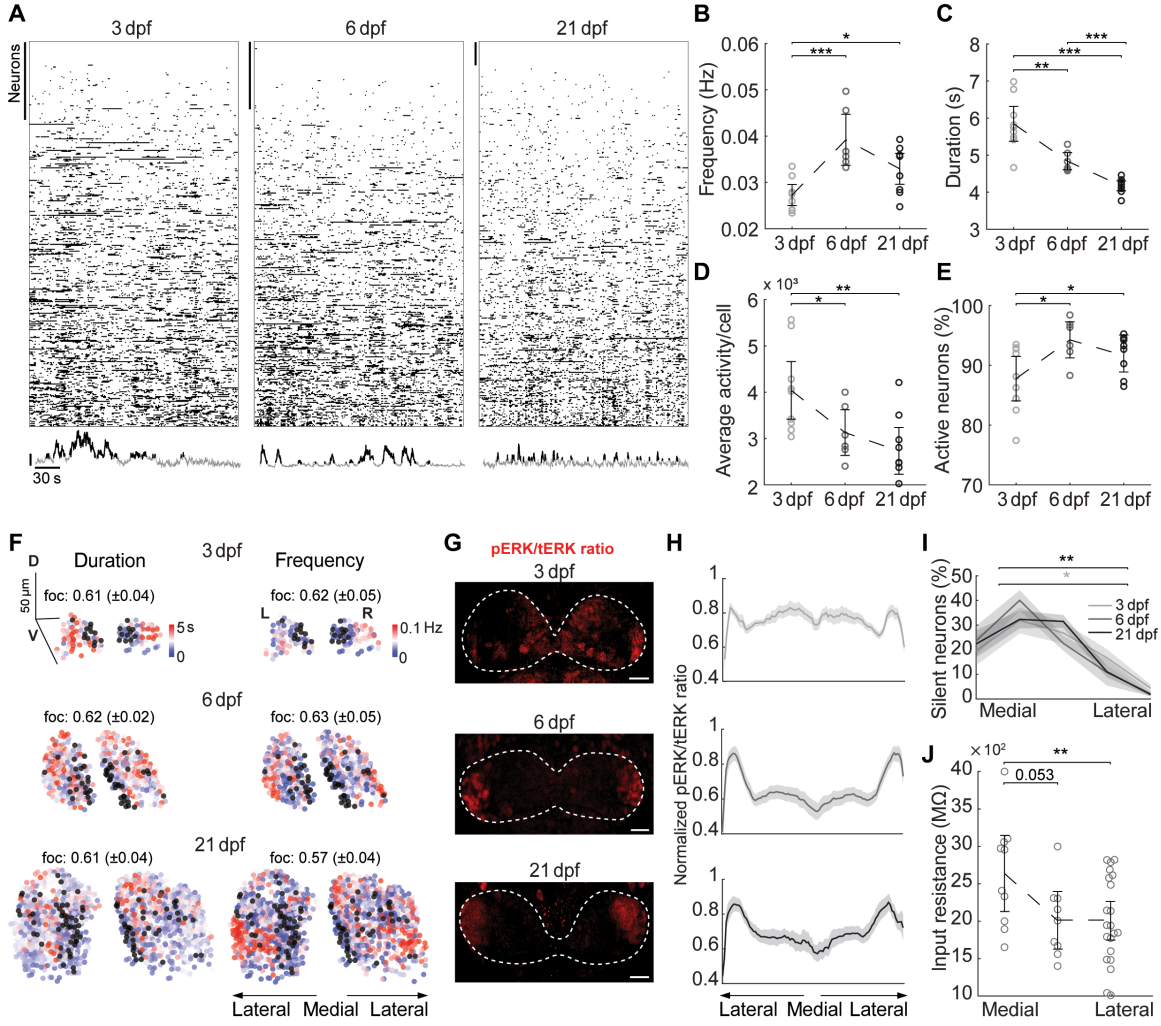

Fig. 6. Features of habenular spontaneous activity change during development. (**A**) Individual spontaneous activity bursts (black markings) detected in all habenular neurons at 3, 6, and 21 dpf sorted on the basis of their increasing overall activity rate. Black bars represent 100 neurons. Bottom panel shows individual examples of spontaneous activity traces from three different neurons, with detected events marked with black color. Black bar represents 10% $\Delta F/F$. (**B**) Average frequency of spontaneous activity bursts in habenular neurons in each zebrafish at 3 dpf ($n = 9$ fish), 6 dpf ($n = 6$ fish), and 21 dpf ($n = 9$ fish). (**C**) Average duration of spontaneous activity bursts in habenular neurons in each zebrafish. (**D**) Average spontaneous activity in habenular neurons in each zebrafish, represented as total area under the curve of all detected events. (**E**) The ratio of spontaneously active neurons with at least one spontaneous activity burst.*$P < 0.05$, **$P < 0.01$, and ***$P < 0.001$, Wilcoxon rank sum test. (**F**) Three-dimensional reconstructions of habenular neurons based on the duration (left) and frequency of their spontaneous activity events. Frequency and duration are color-coded. Black dots are inactive neurons. Coronal view. Scale bars, 50 μm. "foc" represents the focality index as means ± SEM for the temporal features of spontaneous activity bursts, duration, and frequency across all zebrafish and is depicted on top of the individual example's three-dimensional reconstruction. (**G**) Confocal microscopy images of pERK/tERK ratio in representative examples of habenula at 3, 6, and 21 dpf in dorsal view. Scale bars, 20 μm. White dashed lines delineate the borders of habenula. Note the difference in pERK/tERK ratio between medial and lateral ends of habenula. (**H**) Quantifications of the normalized pERK/tERK ratio along the mediolateral axis for each age at 3 dpf ($n = 15$), 6 dpf ($n = 17$), and 21 dpf ($n = 8$). Shading represents SEM. (**I**) The ratio of silent neurons in relation to their normalized mediolateral location along both habenula hemispheres of 3, 6, and 21 dpf. Shading represents SEM. Averages of the two most medial and two most lateral location bins were compared within one age. *$P < 0.05$ for 3 dpf and **$P < 0.01$ for 21 dpf, Wilcoxon signed-rank test. (**J**) Input resistance measured by intracellular recordings of habenular neurons ($n = 40$) across the mediolateral axis of juvenile zebrafish. Medial neurons ($n = 10$), central neurons ($n = 9$), and lateral neurons ($n = 21$) in 14 fish. **$P < 0.01$, Wilcoxon rank sum test. All data are presented as means ± SEM. MΩ, megohms.

experiments also revealed that the number of neurons birthdated at 2.5 dpf was almost double the number of neurons birthdated at 5 dpf (Fig. 7, H and I). This higher rate of habenular neurogenesis at earlier developmental stages is also in line with our observation for a larger number of phospho–histone 3–labeled mitotic cells in habenula at earlier developmental stages (Fig. 7, J to K). Together, our results revealed that sequential neurogenesis in habenula generates spatially organized, nonoverlapping clusters of habenular neurons.

Habenular neurons born at a distinct developmental stage form a distinct functional cluster

Our results in previous sections indicate a potential relationship between the birthdate of habenular neurons, spatial location, and their functional properties. On the basis of these results, we hypothesized that the habenular neurons that are born together might form distinct functional clusters in habenula, with similar features of spontaneous activity. To test this hypothesis, we injected a far-red fluorescence

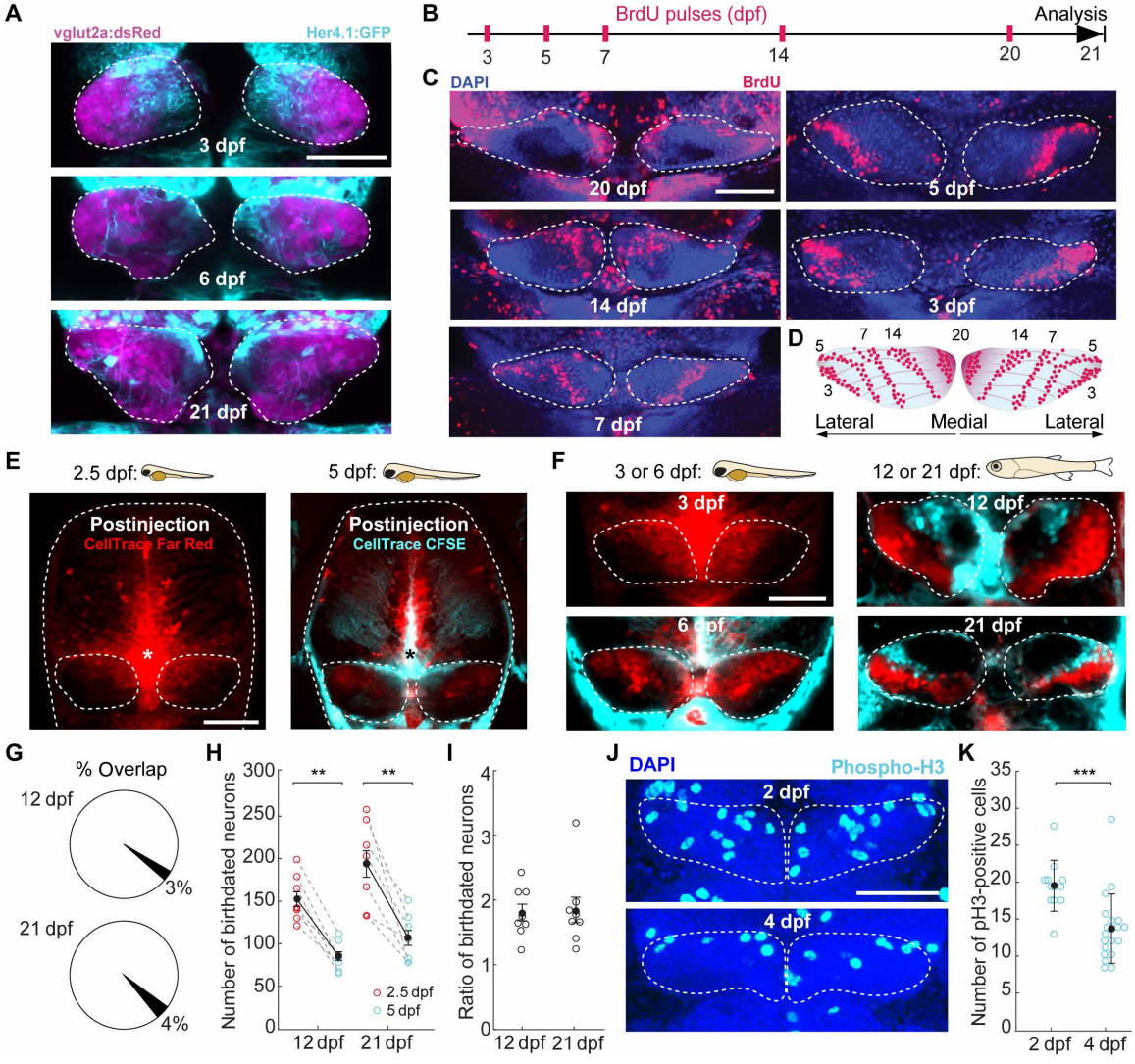

Fig. 7. Distinct spatial domains of habenular neurons are born through sequential neurogenesis. (**A**) Confocal microscopy images of habenula in *Tg(vglut2a:dsRed)* and *Tg(Her4:GFP)* double transgenic zebrafish at 3, 6, and 21 dpf, displaying the glutamatergic neurons (magenta) and potential neuronal progenitors of habenula labeled by Her4 expression (cyan), dorsal view. Scale bar, 50 μm. White dashed lines delineate the borders of habenula. (**B**) Schematic representation of BrdU pulse labeling protocol at 3, 5, 7, 14, and 20 dpf. Animals were raised to 21 dpf before imaging. (**C**) Confocal microscopy images of 21-dpf habenula (white dashed line) showing distribution of neurons that are born at different developmental stages. Neurons were birthdated by using BrdU (red) pulse labeling, at the developmental stages indicated in each panel. DAPI label marks all cells in blue. Dorsal view. Scale bar, 50 μm. (**D**) Schematic representation of the sequential arrangement of neurons that are born at different developmental stages along the mediolateral axis, dorsal view. (**E**) Confocal microscopy images of telencephalic ventricle 15 hours postinjection with CellTrace Far Red (red) at 2.5 dpf (left) and a second injection with CellTrace CFSE (cyan) at 5 dpf (right). Dorsal view. Asterisk shows injection site in the telencephalic ventricle. Borders of the zebrafish telencephalon and habenula are delineated by a dashed white line. Scale bar, 50 μm. (**F**) Confocal microscopy images of habenula 1 day postinjection of CellTrace Far Red (red) injected at 2.5 dpf and CellTrace CFSE (cyan) injected at 5 dpf (left panels). Birthdated habenular neurons are located near the medial wall of the habenula. At 12 and 21 dpf (right panels), habenular neurons labeled at 2.5 and 5 dpf exhibit distinct spatial distributions. Borders of the habenula are delineated by a dashed white line. Scale bar, 50 μm. (**G**) The ratio of overlap between the two populations of habenular neurons birthdated by the sequential injections of Far Red and CFSE cell tracers at 2.5 and 5 dpf, respectively, and quantified at 12 dpf ($n = 8$) and 21 dpf ($n = 8$). (**H**) The number of habenular neurons that were born at 2.5 dpf versus 5 dpf, measured at 12 dpf ($n = 8$) and 21 dpf ($n = 8$). $^{**}P < 0.01$, Wilcoxon rank sum test. (**I**) The ratio of habenular neurons birthdated at 2.5 versus 5 dpf quantified at 12 dpf ($n = 8$) and 21 dpf ($n = 8$). (**J**) Confocal microscopy images of habenula labeled with phospho-H3 antibody (cyan) indicating mitotic cells at 2 and 4 dpf. DAPI label marks all cells in blue. Borders of the habenula are delineated by a dashed white line. Scale bar, 50 μm. (**K**) The number of phospho-H3 positive mitotic cells in the habenula, at 2 and 4 dpf. $^{***}P < 0.001$, Wilcoxon rank sum test. All data are presented as means ± SEM.

cell tracer to the forebrain ventricles of zebrafish larvae expressing GCaMP6s at either 2.5 or 5 dpf (Fig. 8, A and K). Later, we raised these animals to 21 dpf and visualized their habenular activity in the green spectrum while identifying birthdated habenular neurons in the far-red spectrum, by using confocal microscopy (Fig. 8, A and K). Our in vivo birthdating injections at 2.5 or 5 dpf allowed us to classify habenular neurons into distinct spatial zones (Zs), where Z1 represents the earliest born (oldest) neurons and Z2

and Z3 represent later-born neurons with descending order of maturity (Z1 > Z2 > Z3) (Fig. 8, G to Q).

Our analysis revealed notable differences in the functional features of the spontaneous activity between habenular neurons born at different developmental stages, corresponding to distinct spatial zones. Earlier born habenular neurons displayed stronger spontaneous activity (Fig. 8, B, C, L, and M) with higher frequency (Fig. 8, D to N) and duration (Fig. 8E). Moreover, earlier born habenular neurons showed a significantly larger number of pairwise correlations, compared to later-born habenular neurons (Fig. 8, F and P). Our results suggest that distinct functional clusters of habenular neurons with distinct functional features are born at different developmental stages. To test this idea further, we asked whether the developmentally tagged neurons are also related to the spatially organized functional clusters within habenula, observed earlier (Fig. 4, A to D) (*35*). To this end, we clustered the spontaneous habenular activity using k-means clustering (Fig. 8, H, I, R, and S) and calculated the overlap between developmentally tagged neurons and functional clusters, using a "cluster selectivity" index (*35*). If developmentally tagged neurons in different habenular zones overlap with one functional cluster, cluster selectivity would result in 1. We observed that the developmentally tagged habenular neurons in each zone overlap with significantly fewer clusters, when compared to the same number of randomly selected habenular neurons (Fig. 8, J to T). These results revealed that distinct functional clusters of spatially organized habenular neurons are born at distinct developmental stages and exhibit similar features of spontaneous activity.

DISCUSSION

In this study, we investigated the functional development of habenular circuits in zebrafish across development from young larvae with relatively simple behaviors to juvenile zebrafish with complex behaviors (*1*–*3*, *33*, *36*, *37*). The use of juvenile zebrafish is gaining popularity due to their transparent brains and their expanded behavioral repertoire that requires habenular function (*1*–*3*, *37*). Our results revealed that as the zebrafish develop from the larval to the juvenile stage, habenular circuits undergo multiple transitions in its architecture, sensory computations, and intrinsically generated spontaneous activity, which could support the expansion of the behavioral repertoire during development.

Previous studies indicate the presence of olfactory (*34*, *35*) and visual (*23*, *34*) responses in habenula, which were suggested to be involved in generating odor avoidance (*43*) and light preference (*23*). Both visual (*20*) and olfactory (*56*) responses are reported in sensory organs of 2.5-day-old zebrafish larvae. However, the precise developmental maturation of these sensory inputs in habenula has not been investigated. Our results revealed that at early developmental stages, habenula is first innervated by the visual inputs, which are followed by the olfactory inputs. This is also in line with our observation of light responses dominating habenula of larval zebrafish followed by olfactory responses. We observed that aversive mild electric stimulation (*27*, *30*, *37*) elicits responses in habenula during later developmental stages. This gradual increase in stimulus diversity of habenular responses likely reflects a developmental transition of habenula into a multisensory processing brain region, which can encode stimulus salience and valance. We observed that visual, olfactory, vibrational, and electric stimuli are distinctly encoded by the activation of separate neural populations. Such distinct encoding of different sensory modalities at all developmental stages highlights the important role of habenula in integrating information from multiple sensory systems (*23*, *34*, *35*, *43*, *57*). Future experiments are needed to identify the specific role of habenular circuits for distinguishing salience and valance across multiple sensory modalities.

As in other lower vertebrates, zebrafish dHb exhibits prominent molecular (*29*, *30*) and structural asymmetries (*39*). As expected, habenular lateralization has important consequences with respect to the segregation of different sensory modalities across habenular hemispheres and for regulating the targeting of habenular axons to different output regions (*27*, *33*, *39*). We observed that the functional lateralization of sensory inputs and computations in habenula is prominent mostly in the dHb, which develops early during development (*38*), whereas we did not observe functional lateralization in vHb, which develops later (*32*), despite the prominent sensory-evoked vHb responses. This developmental order eventually leads to a decrease in functional lateralization across the entire habenula as the animals maturate. Similar to primary sensory systems (*12*), maturation of zebrafish habenula requires the early presence of sensory inputs (*34*). When these inputs are removed before a critical time window, zebrafish dHb loses its functional lateralization (*34*). It is also important to note that aversive stimuli (mechanical vibrations and mild electric stimulation) did not elicit lateralized responses in zebrafish habenula, which is in line with studies performed in the mammalian lateral habenula, where aversive responses showed no apparent lateralization (*25*, *26*, *58*). We suggest that the apparent lack of lateralization in the mammalian habenula is due to a continued maturation of lateral habenula dominated by aversive cue responses and reduced availability of sensory information during mammalian in utero development.

The activity-dependent maturation of neural circuits does not solely rely on sensory inputs but also includes endogenously generated spontaneous activity (*11*). In several brain regions, spontaneously generated activity is thought to play important roles in the maturation of synaptic connections, refining network topography (*13*, *14*, *59*) and entraining developing circuits (*17*). In our study, we observed that habenular networks exhibit spatially organized spontaneous activity already at early developmental stages. A recent transcriptomics study revealed a topographic organization of habenular neurons based on their distinct molecular features already in 10-day-old zebrafish larvae (*30*) and likely overlap with the spatially organized spontaneous activity studied here. Whether the spontaneous activity is needed for the proper development of distinct habenular clusters or habenular function, as in other brain regions (*13*), is yet to be investigated.

We also observed that temporal features of habenular spontaneous activity changed, leading to faster kinetics at older ages. The trend for faster kinetics of intrinsically generated activity across development was also observed in other higher brain regions, such as the hippocampus (*16*, *50*). What may underlie the faster kinetics of spontaneous activity bursts in older ages? It is likely that multiple processes can modulate spontaneous habenular activity leading to the observed dynamical changes during development. One possibility is that early spontaneous activity might be driven by glia (*20*) or other support cells (*21*), which usually generate slow bursts of activity. It was previously shown that astrocytes can modulate the bursting activity in the rodent habenula (*60*), and astroglia activation in

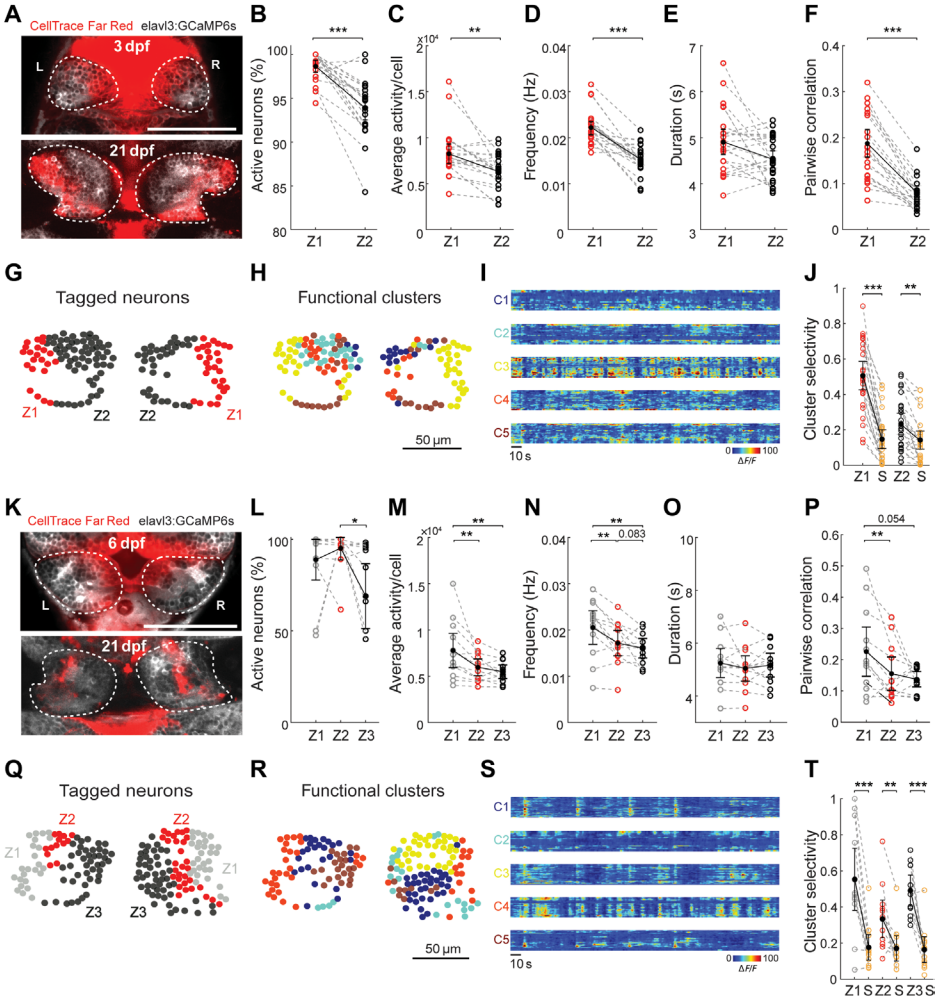

Fig. 8. Habenular neurons that are born at a distinct developmental stage exhibit similar functional properties. (**A**) Confocal microscopy images of *elavl3:GCaMP6s* (white) zebrafish habenula at 3 (top) and 21 (bottom) dpf, after the injection of the CellTrace Far Red (red) at 2.5 dpf. Dorsal view. Habenula is delineated by a dashed white line. Developmentally tagged, red-labeled neurons at 21 dpf are in zone 1 (Z1 = early born), whereas unlabeled neurons are in zone 2 (Z2 = later born). Scale bar, 100 µm. L, left; R, right. (**B**) The ratio of spontaneously active Z1 (red) versus Z2 (black) habenular neurons at 21 dpf. Note that a higher ratio of early-born habenular neurons in Z1 are active, when compared to later-born neurons in Z2 ($n = 21$ planes in 12 fish). (**C**) Average spontaneous activity that is represented as total area under the curve of all detected events, in Z1 versus Z2 habenular neurons at 21 dpf. (**D**) Average spontaneous activity burst frequency in Z1 versus Z2 habenular neurons at 21 dpf. (**E**) Average spontaneous activity burst duration in Z1 versus Z2 habenular neurons at 21 dpf. (**F**) Average pairwise correlations of Z1 versus Z2 habenular neurons at 21 dpf. Note that Z1 neurons are significantly more correlated than Z2 habenular neurons. $^{**}P < 0.01$ and $^{***}P < 0.001$, Wilcoxon signed-rank test. (**G**) Spatial distribution of labeled early-born (Z1) versus later-born (Z2) habenular neurons, in an example zebrafish at 21 dpf. (**H**) Spatial distribution of habenular neurons color-coded according to their functional clusters based on their spontaneous activity, using k-means clustering in the same example zebrafish as in (I). (**I**) Color-coded neural traces showing the spontaneous activity of each habenular neuron that belong to a given cluster "C," in the same example zebrafish as (G) and (H). Warm colors represent increased neural activity. Note the prominent overlap between the functional cluster C3 (yellow neurons in H) and Z1 neurons in (G). (**J**) Cluster selectivity of Z1 versus Z2 habenular neurons, when compared to the same number of randomly selected habenular neurons (S) in yellow. Note that both Z1 and Z2 habenular neurons belong to fewer functional clusters compared to an equal number of random neurons. $^{**}P < 0.01$, Wilcoxon signed-rank test. Also, note that Z1 neurons are significantly more cluster selective than Z2. $^{***}P < 0.001$, Wilcoxon rank sum test. (**K**) Confocal microscopy images of *elavl3:GCaMP6s* (white) zebrafish habenula at 5 (top) and 21 (bottom) dpf, after the injection of the cell tracer (red) at 5 dpf. Oldest neurons (Z1 = early born) are located lateral to the red-labeled neurons (Z2 = intermediate born) that are developmentally tagged at 5 dpf. The youngest neurons (Z3 = late born) are located medial to the red-labeled neurons. Scale bar, 100 µm. L, left; R, right. (**L**) The ratio of spontaneously active Z1 (gray), Z2 (red), and Z3 (black) habenular neurons at 21 dpf ($n = 12$ planes in five fish). Note that a higher ratio of Z2 neurons are active, when compared to Z3 neurons. (**M**) Average spontaneous activity that is represented as total area under the curve of all detected events, in Z1, Z2, and Z3 habenular neurons at 21 dpf. (**N**) Average spontaneous activity burst frequency in Z1, Z2, and Z3 habenular neurons at 21 dpf. (**O**) Average spontaneous activity burst duration in Z1, Z2, and Z3 habenular neurons at 21 dpf. (**P**) Average pairwise correlations of Z1, Z2, and Z3 habenular neurons at 21 dpf. $^{**}P < 0.01$, Wilcoxon signed-rank test. (**Q**) Spatial distribution of early-born (Z1), intermediate-born (Z2), and later-born (Z3) habenular neurons, in an example zebrafish at 21 dpf. (**R**) Spatial distribution of habenular neurons color-coded according to their functional clusters based on their spontaneous activity, using k-means clustering in the same example zebrafish as in (I). (**S**) Color-coded neural traces showing the spontaneous activity of each habenular neuron that belong to a given cluster "C," in the same example zebrafish as (G) and (H). Warm colors represents increased neural activity. (**T**) Cluster selectivity of Z1, Z2, and Z3 habenular neurons, when compared to the same number of randomly selected habenular neurons (S) in yellow. Note that Z1, Z2, and Z3 habenular neurons belong to fewer functional clusters compared to equal number of random neurons. $^{***}P < 0.001$, Wilcoxon signed-rank test. All data are presented as means ± SEM.

zebrafish can excite nearby neurons (*61*). Alternatively, it is possible that as the habenula develops, synaptic connections between habenular neurons become more mature. Together with the increased inhibition we observed in the habenula, by the addition of GABAergic connections, such mature synapses can support faster neural dynamics. Last, part of the habenular spontaneous activity might also be driven by the activation of the ancestral corticolimbic homologs in the zebrafish forebrain. For example, it was shown that habenula is strongly driven by inputs received from entopeduncular nucleus (*24*, *62*), lateral hypothalamus (*26*), and cortex (*58*). Hence, it is likely that the homologs of these input regions are not yet fully developed and cannot drive habenular activity in young zebrafish larvae. A recent study showed that the zebrafish equivalent of amygdala (Dm) (*63*), driving both entopeduncular nucleus and lateral hypothalamus (*63*), also develops during the late juvenile stage (*64*). Together, we suggest that all these processes jointly contribute to the habenular spontaneous activity.

Our results revealed that the developmental changes in the temporal kinetics of habenular spontaneous activity are accompanied by the sequential addition of newborn neurons across development. More specifically, we found that the spatially confined locations of neuronal clusters that are born during distinct developmental stages follow a mediolateral arrangement. In this arrangement, youngest neurons are located closer to the neural progenitors of the habenula on the medial wall, while the oldest habenular neurons are located closer to the lateral wall. Similar sequential stacking of newly born neurons was also observed during forebrain development in both zebrafish (*65*, *66*) and rodents (*6*, *67*). Moreover, such a sequential order of neurogenesis contributes to different neural subtypes in the zebrafish hindbrain and spinal cord (*8*–*10*), as well as the rodent entorhinal cortex (*5*). Hence, it is possible that recently described populations of habenular neurons with distinct molecular identities (*30*) might be born during different developmental stages of the zebrafish habenula. The topographically organized molecular (*30*) and functional clusters (*30*, *35*, *37*) of habenular neurons represent the distinct subdomains or functional modules of habenula and are likely associated with different aspects of animal behavior. Our data revealed that at least two of the functional clusters within habenula are born at two different developmental stages, stay in spatially confined locations, and exhibit different functional features. Therefore, we propose that the distinct functional clusters of habenular neurons are born at different developmental time points. In turn, such a developmental order could contribute to an increased diversity of habenular neurons and expand habenular function across development. These ideas are in line with several recent studies that suggest that complex and cognitively demanding behaviors arise later in development as animals maturate (*1*, *2*, *33*, *37*). Our findings in habenula suggest that such expansion of animal behavior might be due to the incorporation of new functional modules at different developmental time points. In the future, it will be interesting to see whether such sequential addition of new neuronal modules with distinct functional properties is a feature that is not only unique to habenula but also preserved across the brain.

MATERIALS AND METHODS

Fish maintenance

The animal facilities and maintenance of zebrafish, *Danio rerio*, were approved by the Norwegian Food Safety Authority. Fish were kept in 3.5-liter tanks at a density of 15 to 20 fish per tank in a Techniplast Zebtech Multilinking system at 28°C (pH 7), 6.0 ppm O_2, and 700 μS, at a 14-hour light/10-hour dark cycle. Fish received a normal diet of dry food (Zebrafeed, Sparos) two times per day and *Artemia nauplii* once a day (Grade 0, Platinum Label, Argent Laboratories). Larvae were maintained in egg water (1.2 g of marine salt and 0.1% methylene blue in 20 liters of reverse osmosed water) from fertilization to 3 dpf. From 3 to 6 dpf, larvae were kept in artificial fish water (AFW): 1.2 g of marine salt in 20 liters of RO water. Animals used for experiments at 21 dpf were transferred to 3.5-liter tanks in the zebrafish facility at 3 dpf.

For experiments, the following fish lines were used: *Tg(elavl3:GCaMP6s)* (*41*), *Tg(gad1b:GFP)* (*42*), *Tg(vglut2a:dsRed)* (*22*), *Tg(Lhx2a:gap-YFP)* (*22*), *Et(−0.6hsp70l:Gal4-VP16) s1020t; UAS:nfsB-mCherry* (*44*), and *Tg(her4.1:GFP)* (*53*). Experiments were performed on embryos of nacre [*mitfa*; (*68*)] background.

Confocal anatomical imaging

Before embedding, fish were anesthetized with 0.02% tricaine methanesulfonate (MS-222). Animals were then embedded in 1% (for 3 to 6 dpf) or 2% (for 21 dpf) low–melting point (LMP) agarose (Thermo Fisher Scientific) in a recording chamber (FluoroDish, World Precision Instruments) with AFW. Anatomical *Z* scans were acquired using a Zeiss Examiner Z1 confocal microscope with a 20× water immersion objective [Zeiss; numerical aperture (NA) of 1.0; Plan-Apochromat] at room temperature, using 4× to 10× average for each plane.

BrDU labeling, immunostaining, and imaging

Labeling of newborn neurons with BrdU was performed at 3.5, 5.5, 7.5, 14.5, and 20.5 dpf in *Tg(HuC:GFP)* (*69*) fish outcrossed to wild-type (AB) fish. Embryos (25 hours post-fertilization) were dechorionated by Proteinase K (0.1 mg/ml; catalog number 25530049) at room temperature and washed several times with 1× E3 medium. A stock of 10 mM BrdU (Sigma-Aldrich, catalog number B5002) in 1× E3 medium was prepared, aliquoted, and stored at −20°C until use. For each treatment, a final concentration of 500 μM BrdU was applied to 3- and 5-dpf fish. For 7-, 14-, and 21-dpf fish, 2.5 mM BrdU was used. Treatments were all performed for 5 hours. Fish were kept in a dark incubator until 5 dpf and were transferred to the water system at 6 dpf. From this point on, a 14-hour light/10-hour dark cycle was maintained. At 22 dpf, fish were sacrificed and fixed in 4% paraformaldehyde (PFA) to 1% dimethyl sulfoxide (DMSO) at +4°C overnight, washed with 0.8% Triton X-100 in 1× phosphate-buffered saline (PBS; PBSTx), dehydrated by a serial methanol gradient, and kept at −20°C until further use. For immunohistochemical staining, fish were rehydrated back to the aqueous phase (1× PBS). Brains were dissected out in cold 1× PBS and were incubated in precooled acetone for 10 min at −20°C. Brains were incubated in preheated 2 mM HCl at 37°C for 12 min, cooled at room temperature for 10 min, and washed with 0.8% PBSTx. Samples were incubated in Rat anti-BrdU immunoglobulin G (IgG; 1:200 Bio-Rad, catalog number MCA2060) monoclonal antibody overnight at +4°C. After serial washes in 0.8% PBSTx, the secondary antibody (Goat anti-rat Alexa 555; 1:500 dilution; Thermo Fisher Scientific, catalog numberA-21434) and 4′,6-diamidino-2-phenylindole (DAPI) at 1:3000 dilution were applied. Following an overnight incubation at +4°C, samples were washed for a total of 2 hours with 0.8% PBSTx.

To measure pERK/tERK ratio, fish were euthanized and fixed in cooled 4% PFA in 0.25% PBTx (0.25% Triton X-100 in 1× PBS)

overnight at 4°C. Samples were permeabilized in 0.50% Trypsin-EDTA on ice for 40 min and washed. The samples were then incubated in the blocking solution [2% normal goat serum, 1% bovine serum albumin (BSA), and 1% DMSO in 0.25% PBTx] for 1 hour followed by incubation in primary antibody solution [1:500 antibody (Ab), 1% BSA, and 1% DMSO in 0.25% PBTx] overnight at 4°C. Next, samples were washed and incubated with secondary antibody solution (1:1000 Ab, 1:1000 DAPI, 1% BSA, and 1% DMSO in 0.25% PBTx) overnight at 4°C. Last, samples were washed and placed in glycerol. pERK/tERK ratio of the median *z*-projection confocal images were calculated in ImageJ (Fiji). The pERK/tERK ratio is normalized by the maximum pERK/tERK ratio and adjusted for the habenular size using a custom-made script in MATLAB.

For phospho–histone 3 staining, larvae were fixed in 4% PFA for 2 hours at room temperature or overnight at 4°C. Following washes in 0.3% Triton-X in PBS (0.3% PBSTx), fixed samples were permeabilized in 100% acetone at −20°C for 20 min and blocked in 0.3% PBSTx containing 0.1% BSA. Samples were incubated with the primary antibody (phospho–histone 3, Santa Cruz Biotechnology, #sc-8656-R; 1:500 dilution) overnight at +4°C, followed by serial washes in 0.3% PBSTx and incubation with the secondary antibody (goat anti-rabbit Alexa 488 plus, Thermo Fisher Scientific, #A-11034, 1:1000 dilution) overnight at +4°C. Next, samples were incubated in DAPI (1:1000) for 2 hours, before serial washes in 0.3% PBSTx.

For preservation, samples were transferred to 80% glycerol in 1× PBS and were kept at +4°C in the dark. For imaging, labeled brains were mounted in 80% glycerol on a glass slide with a coverslip. Anatomical *Z* scans of habenula were acquired using a Zeiss Examiner Z1 confocal microscope with a 20× plan NA 0.8 objective, using 2× to 10× average for each plane. Phospho–histone 3–positive cells were manually counted on confocal stack using the Cell Counter Plugin of Fiji/ImageJ.

In vivo two-photon calcium imaging and sensory stimulation

Two-photon calcium imaging was performed on 3-, 6-, and 21-dpf-old *Tg(elavl3:GCaMP6s)* zebrafish. Before embedding, fish were anesthetized with cold AFW. Animals were then embedded in 1% (for 3 to 6 dpf) and 2% (for 21 dpf) LMP agarose (Thermo Fisher Scientific) in a recording chamber (FluoroDish, World Precision Instruments). LMP agarose solidified for 20 min, and the section covering the nose was carefully removed to expose the nostrils. The animal was then placed under the microscope with constant perfusion of AFW bubbled with carbogen (95% O_2 and 5% CO_2). First, spontaneous activity was measured for 30 min. Afterward, five repetitions of sensory stimuli (red light flash or food odor) were applied. The food odor stimulus was prepared by adding 1 g of standard dried fish food (Zebrafeed, Sparos; <100) in 50 ml of AFW, dissolved for 1 hour, filtered with a 22-μm filter, and diluted 1:50 in AFW. For skin extract (*70*), an adult zebrafish was euthanized in ice-cold water and decapitated, and the skin was peeled off from the body, incubated in 1 ml of AFW, mixed, and centrifuged at 1300 rpm and 4°C for 1 hour. One milliliter of the supernatant was then dissolved in 300 ml of AFW. Amino acid mixture (*70*) contained arginine, asparagine, aspartic acid, alanine, phenylalanine, histidine, and methionine, all diluted in AFW at 10^{-4} M final concentration. Ammonium chloride was diluted in AFW at 10^{-4} M final concentration. The odor stimulus was delivered for 5 s through a tube positioned in the front of the fish, connected to an Arduino Due–controlled high-performance liquid chromatography injection valve (Valco Instruments). Fluorescein (10^{-4} M) was dissolved in AFW and used to measure the precise onset of odor delivery to the nose at the end of each experiment. For the light stimulus, we used a red LED (LZ1-00R105, LedEngin; 625-nm wavelength) and placed it in the front of the recording chamber near the tube. The light stimulus was a flash of 2-s duration with an intensity of 0.318 mW. Mechanical vibrations were delivered via solenoid tapper (SparkFun Electronics, ROB-10391), via 50-ms application of 6 V. Mild electric stimulation was delivered by tungsten electrodes that passed 1-kHz oscillating current of 0.05 mA for a period of 1 s. The recordings were performed with a two-photon microscope (Scientifica) using a 16× water immersion, long working-distance objective (Nikon, NA 0.8, LWD 3.6). A mode-locked Ti:Sapphire laser (MaiTai Spectra-Physics) tuned to 920 nm was used for excitation. Volumetric recordings (eight planes with Piezo) were obtained at an acquisition rate of 31.9 Hz for a volume of 1536 × 512 pixels × 8 planes. Total duration of the recordings was 45 to 60 min.

Juvenile zebrafish electrophysiological recordings of habenular neurons

The experiments were conducted in a juvenile zebrafish brain explant preparation (*61*). Juvenile zebrafish were euthanized by immersion in ice-cold water, followed by decapitation to ensure death. The head was transferred in cold artificial cerebrospinal fluid (ACSF) bubbled with carbogen (95% O_2/5% CO_2). The ACSF (*70*) was composed of the following chemicals diluted in reverse-osmosis purified water: 131 mM NaCl, 2 mM KCl, 1.25 mM KH_2PO_4, 2 mM $MgSO_4{\cdot}7H_2O$, 10 mM glucose, 2.5 mM $CaCl_2$, and 20 mM $NaHCO_3$. The eyes, jaws, and ventral part of the skull were carefully removed using forceps, exposing the habenula. The brain explant was then affixed using tungsten pins to a small petri dish coated with Sylgard (World Precision Instruments) and perfused in constant flow bubbled ACSF.

We performed intracellular recordings of single habenular neurons, via borosilicate patch pipettes (10 to 12 megohms) mounted on a MultiClamp 700B amplifier. Electrodes contained the intracellular solution (130 mM k-gluconate, 10 mM Na-gluconate, 10 mM Hepes, 10 mM Na^{2+}-phosphocreatine, 4 mM NaCl, 4 mM adenosine 5′-triphosphate–Mg, and 0.3 mM Na^{3+}-GTP) (*70*). Negative voltage steps (−30 mV) of 500 ms were applied to measure the input resistance.

In vivo birthdating of neurons

Before injections, 2.5-dpf larvae were dechorionated manually and anesthetized in 0.01% MS-222 in AFW for 5 to 10 min. Injections were done on larvae embedded in 1% LMP agarose in AFW and 0.01% MS-222 in AFW. The stock solution contained 5 mM CellTrace Far Red–AM or CellTrace CFSE Cell Proliferation Kit (Thermo Fisher Scientific) dissolved in DMSO provided with the proliferation kit. The injection mixtures contained 0.5 μl of this CellTrace Far Red/DMSO stock solution dissolved in 2.5 μl of ACSF with a final concentration of 1 mM. The ACSF contained the following: 124 mM NaCl, 22 mM D-(+)-glucose, 2.0 mM KCl, 1.6 mM $MgSO_4{\cdot}7\ H_2O$, 1.3 mM KH_2PO_4, 24 mM $NaHCO_3$, and 2.0 mM $CaCl_2{\cdot}2H_2O$. The injection needles were pulled with a Sutter Instrument Co. Model P-2000, from thin-walled borosilicate capillaries (1.00 mm; VWR), with the following settings: heat = 785, filament = 4, velocity = 40, delay = 220, and pull = 70. The needle tip was cut open with forceps afterward, and a pressure injector (Eppendorf Femtojet 4i) was used

Table 1. Key resource table presenting the source and identifier of chemicals, transgenic lines, and materials.

Reagent or resource	Source	Identifier
Chemicals		
MS222 (tricaine methanesulfonate)	Sigma-Aldrich	Catalog number E10521
LMP agarose	Thermo Fisher Scientific	Catalog number 16520100
PBS	Thermo Fisher Scientific	Catalog number BR0014G
CellTrace Far Red Cell Proliferation Kit	Thermo Fisher Scientific	Catalog number C34564
CellTrace CFSE Cell Proliferation Kit	Thermo Fisher Scientific	Catalog number C34554
Proteinase K	Thermo Fisher Scientific	Catalog number 25530049
BrdU	Sigma-Aldrich	Catalog number B5002
Triton-X	Sigma-Aldrich	Catalog number T8787
DMSO	Sigma-Aldrich	Catalog number D8418
Rat anti-BrdU	Bio-Rad	Catalog number MCA2060
Rabbit anti-phosphoh3	Santa Cruz Biotechnology	Catalog number sc-8656-R
Goat anti-rat Secondary Antibody, Alexa 555	Thermo Fisher Scientific	Catalog number A-21434
Goat anti-rabbit Secondary Antibody, Alexa 488 plus	Thermo Fisher Scientific	Catalog number A-11034
p44/42 MAPK Mouse mAb	Cell Signaling Technology	Catalog number 4696
Phospho-p44/42 MAPK Rabbit mAb	Cell Signaling Technology	Catalog number 4370
Goat anti-Mouse IgG Secondary Antibody, Alexa Fluor Plus 488	Thermo Fisher Scientific	Catalog number A32723
Zebrafish lines	**Source and brief description**	
Tg(elavl3:GCaMP6s)	(*41*) Expresses GCaMP6s panneuronally	ZFIN catalog number ZDB-ALT-141023-1, RRID:ZFIN_ZDB-ALT-141023-1
Tg(gad1:GFP)	(*42*) Expresses GFP in GABAergic neurons	ZFIN catalog number ZDB-ALT-131127-6, RRID:ZFIN_ZDB-ALT-131127-6
Tg(vglut2a:dsRed)	(*22*) Expresses dsRed in glutamatergic neurons	ZFIN catalog number ZDB-ALT-100505-2, RRID:ZFIN_ZDB-ALT-100505-2
Tg(lhx2a:gap-YFP)	(*22*) Expresses membrane tagged YFP in mitral cells	ZFIN catalog number ZDB-ALT-100504-12, RRID: ZFIN_ZDB-ALT-100504-12
Et(−0.6hsp70l:Gal4-VP16) s1020t	(*44*) Expresses Gal4 in thalamic neurons	ZFIN catalog number ZDB-ALT-070420-21, RRID: ZFIN_ZDB-ALT-070420-21
Tg(UAS: nfsB-mCherry)	(*44*) Expresses *UAS:nfsB-mCherry* ubiquitously (*44*)	Catalog number ZFIN ZDB-ALT-070316-1, RRID: ZFIN_ZDB-ALT-070316-1
Tg(her4.1: GFP)	(*53*) Expresses GFP in neural progenitors	ZFIN catalog number ZDB-ALT-070612-3, RRID: ZFIN_ZDB-ALT-070612-3
Software and algorithms		
ImageJ/Fiji	https://fiji.sc/	
Cell detection, image alignment, and processing	(*35*, *61*, *71*)	
Event detection	(*51*)	
Other		
Pressure injector	Eppendorf	Femtojet 4i
Confocal microscope (20× plan NA 0.8 objective)	Zeiss	Examiner Z1
Stereomicroscope (20× Plan-Apochromat, NA 0.8)	Zeiss	Axio Imager M1
Two-photon microscope	Scientifica	
Sutter laser puller	Sutter	Model P-200
Solenoid tapper	SparkFun Electronics	ROB-10391

to inject 1 nl of solution in the telencephalic ventricle near habenula of either 2.5- or 5-day-old zebrafish larvae (*55*). The pressure and time used for the injection were calibrated for each needle using a 0.01-mm calibration slide for microscopy. Usually, the pressure ranged between 100 and 150 hPa, and the time span of the pressure pulse lasted for 0.30 to 0.70 s. After injection, fish were released from agarose and recovered at 28°C AFW and transferred to the fish facility and raised until 12 or 21 days.

Fish (21 dpf) were prepared for confocal microscopy imaging as described above for two-photon calcium imaging. Imaging was performed using a Zeiss Examiner Z1 confocal microscope with a 20× water immersion objective (Zeiss; NA of 1.0; Plan-Apochromat) at room temperature and constant perfusion of AFW bubbled with carbogen (95% O_2 and 5% CO_2). In vivo calcium recordings of the spontaneous activity in habenula were acquired at an acquisition rate of 1.918 Hz for 512 × 1024 pixels during 5 min.

Data analysis

Two-photon microscopy images were aligned using an adapted algorithm (*71*) that corrects for occasional drift in the *XY* dimension, based on "hierarchical model-based motion estimation" (*72*). Every recording was manually checked for motion, and corresponding frames were discarded from further analysis. Individual neurons were semiautomatically detected using a pattern recognition algorithm as previously described (*35*, *61*, *71*). Once neurons were detected, their locations were individually tracked during the recording. If any z-motion drift or if some detected neurons were no longer visible, those neurons were discarded from further analysis. The pixels belonging to each neuron were then averaged providing the complete time course of each neuron over time. The same cell-detection algorithms were used for the confocal recordings in Fig. 6. To distinguish between developmentally tagged and untagged neurons, we manually identified the red cells. To normalize the spontaneous activity for each cell to its baseline fluorescence, we calculated the fractional change in fluorescence ($\Delta F/F$) relative to the baseline, which was calculated as the eighth percentile of activity observed within a 2-min time window as previously described (*51*). Clustering of neurons was performed as previously reported on the basis of the k-means clustering algorithm in MATLAB, as well as the calculation of cluster fidelity and cluster selectivity for sensory and tagged cells (*35*).

Before event detection, traces from neurons in the two-photon recordings were resampled to a final rate of 2 Hz (using decimate function in MATLAB), to match the sampling rate with confocal experiments. Significant calcium events were detected using an algorithm (*51*) that detects calcium events significantly different from noise level within a 95% confidence interval. A cell was considered active if at least one event was detected in 4 min of ongoing activity. The amplitude of events was defined as the maximum peak in the event. The average activity per cell was defined as the sum of the area under the curve (using trapezoidal numerical integration method, function "trapz" in MATLAB) for all events within one neuron. The fractional change in fluorescence ($\Delta F/F$) for the odor and light stimulus, as well as mechanical vibrations and mild electric stimulus, was calculated by subtracting the average baseline fluorescence before stimulus onset (5 s) from the responsive window (10 s for odor and 2 s for light, mechanical vibrations, and mild electric stimulus from the onset of the stimulus). Cells were classified as responding if at least four out of five trials showed the same sign difference (+/−) locked to the stimulus onset. Only the positively responding neurons were taken into account for further analysis.

The focality index was calculated as 1 minus the average of the Euclidean distances between the top 10% neurons (with highest frequencies or durations) divided by the average of the Euclidean distances of all neurons within each hemisphere. The average focality index per fish was calculated by taking the average over the two hemispheres. Same focality index was calculated for the sensory-responding cells.

Cluster fidelity was calculated by measuring the probability of pairs of neurons being in the same cluster during two different time periods (*35*). As a control, we shuffled the cluster identity of neurons randomly.

To calculate cluster selectivity, we first calculated the cluster identity of each neuron using k-means clustering of spontaneous neural activity (*35*). Later, we identified neurons with a given property, in this case, either sensory responding neurons (Fig. 4G) or developmentally tagged neurons (Fig. 6L), and measured the sparseness in the distribution of identified neurons into clusters (*35*). We then compared this to all and/or equal number of nonsensory responding neurons within each fish. If sparseness is 1, all identified neurons are selectively members of a single cluster; if sparseness is 0, all identified neurons are equally distributed into all functional clusters identified by k-means clustering.

The lateralization index was calculated as the difference between the percentage of responding neurons in the left and right hemispheres. If lateralization index is 1, neurons are lateralized to one hemisphere; if lateralization index is 0, neurons are equally distributed among hemispheres.

In the confocal microscopy functional imaging, results for frequency, duration, number of active neurons, average activity, and pairwise correlations are shown for all planes imaged in each fish. These recordings were done at different time points.

Quantification and statistical analysis

Statistical analysis was done using MATLAB, and *P* values are indicated in the figure legends (*$P < 0.05$, **$P < 0.01$, and ***$P < 0.001$). Student *t* test was used for paired data, and unpaired *t* test was used when data were obtained from two independent datasets. For the data that displayed no Gaussian distribution, we used Wilcoxon signed-rank test for paired data and Wilcoxon rank sum test for unpaired data.

Data and software

All analysis was performed with Fiji and MATLAB as indicated in Results.

Key resource table

Table 1 shows the source and identifier of chemicals, transgenic lines, and materials used in the study.

SUPPLEMENTARY MATERIALS

Supplementary material for this article is available at http://advances.sciencemag.org/cgi/content/full/6/36/eaaz3173/DC1

View/request a protocol for this paper from *Bio-protocol*.

REFERENCES AND NOTES

1. A. Valente, K.-H. Huang, R. Portugues, F. Engert, Ontogeny of classical and operant learning behaviors in zebrafish. *Learn. Mem.* **19**, 170–177 (2012).
2. Palumbo, F., Serneels, B., Pelgreems, R., Yaksi, E., The zebrafish dorsolateral habenula is required for updating learned behaviors. bioRxiv, *in revision* Cell Reports, 2020: p. 802256.
3. E. Dreosti, G. Lopes, A. R. Kampff, S. W. Wilson, Development of social behavior in young zebrafish. *Front. Neural Circuits* **9**, 39 (2015).

4. E. A. Brenowitz, M. D. Beecher, Song learning in birds: Diversity and plasticity, opportunities and challenges. *Trends Neurosci.* **28**, 127–132 (2005).
5. F. Donato, R. I. Jacobsen, M.-B. Moser, E. I. Moser, Stellate cells drive maturation of the entorhinal-hippocampal circuit. *Science* **355**, eaai8178 (2017).
6. E. S. Lein, T. G. Belgard, M. Hawrylycz, Z. Molnár, Transcriptomic perspectives on neocortical structure, development, evolution, and disease. *Annu. Rev. Neurosci.* **40**, 629–652 (2017).
7. S. Mayer, J. Chen, D. Velmeshev, A. Mayer, U. C. Eze, A. Bhaduri, C. E. Cunha, D. Jung, A. Arjun, E. Li, B. Alvarado, S. Wang, N. Lovegren, M. L. Gonzales, L. Szpankowski, A. Leyrat, J. A. A. West, G. Panagiotakos, A. Alvarez-Buylla, M. F. Paredes, T. J. Nowakowski, A. A. Pollen, A. R. Kriegstein, Multimodal single-cell analysis reveals physiological maturation in the developing human neocortex. *Neuron* **102**, 143–158.e7 (2019).
8. M. Koyama, A. Kinkhabwala, C. Satou, S.-i. Higashijima, J. Fetcho, Mapping a sensory-motor network onto a structural and functional ground plan in the hindbrain. *Proc. Natl. Acad. Sci. U.S.A.* **108**, 1170–1175 (2011).
9. A. Pujala, M. Koyama, Chronology-based architecture of descending circuits that underlie the development of locomotor repertoire after birth. *eLife* **8**, e42135 (2019).
10. D. L. McLean, J. R. Fetcho, Spinal interneurons differentiate sequentially from those driving the fastest swimming movements in larval zebrafish to those driving the slowest ones. *J. Neurosci.* **29**, 13566–13577 (2009).
11. A. A. Penn, C. J. Shatz, Brain waves and brain wiring: The role of endogenous and sensory-driven neural activity in development. *Pediatr. Res.*, **45** (4 Pt 1), 447–458 (1999).
12. T. N. Wiesel, D. H. Hubel, Comparison of the effects of unilateral and bilateral eye closure on cortical unit responses in kittens. *J. Neurophysiol.* **28**, 1029–1040 (1965).
13. V. Moreno-Juan, A. Filipchuk, N. Antón-Bolaños, C. Mezzera, H. Gezelius, B. Andrés, L. Rodríguez-Malmierca, R. Susín, O. Schaad, T. Iwasato, R. Schüle, M. Rutlin, S. Nelson, S. Ducret, M. Valdeolmillos, F. M. Rijli, G. López-Bendito, Prenatal thalamic waves regulate cortical area size prior to sensory processing. *Nat. Commun.* **8**, 14172 (2017).
14. L. C. Kat, C. J. Shatz, Synaptic activity and the construction of cortical circuits. *Science* **274**, 1133–1138 (1996).
15. Y. Ben-Ari, Developing networks play a similar melody. *Trends Neurosci.* **24**, 353–360 (2001).
16. X. Leinekugel, I. Khalilov, Y. Ben-Ari, R. Khazipov, Giant depolarizing potentials: The septal pole of the hippocampus paces the activity of the developing intact septohippocampal complex in vitro. *J. Neurosci.* **18**, 6349–6357 (1998).
17. S. Gretenkord, J. K. Kostka, H. Hartung, K. Watznauer, D. Fleck, A. Minier-Toribio, M. Spehr, I. L. Hanganu-Opatz, Coordinated electrical activity in the olfactory bulb gates the oscillatory entrainment of entorhinal networks in neonatal mice. *PLOS Biol.* **17**, e2006994 (2019).
18. M. Meister, R. O. Wong, D. A. Baylor, C. J. Shatz, Synchronous bursts of action potentials in ganglion cells of the developing mammalian retina. *Science* **252**, 939–943 (1991).
19. R. Yuste, A. Peinado, L. C. Katz, Neuronal domains in developing neocortex. *Science* **257**, 665–669 (1992).
20. R.-w. Zhang, W.-j. Du, D. a. Prober, J.-L. Du, Muller glial cells participate in retinal waves via glutamate transporters and AMPA receptors. *Cell Rep.* **27**, 2871–2880.e2 (2019).
21. T. A. Babola, S. Li, A. Gribizis, B. J. Lee, J. B. Issa, H. C. Wang, M. C. Crair, D. E. Bergles, Homeostatic control of spontaneous activity in the developing auditory system. *Neuron* **99**, 511–524.e5 (2018).
22. N. Miyasaka, K. Morimoto, T. Tsubokawa, S.-i. Higashijima, H. Okamoto, Y. Yoshihara, From the olfactory bulb to higher brain centers: Genetic visualization of secondary olfactory pathways in zebrafish. *J. Neurosci.* **29**, 4756–4767 (2009).
23. B.-b. Zhang, Y.-y. Yao, H.-f. Zhang, K. Kawakami, J.-l. Du, Left habenula mediates light-preference behavior in zebrafish via an asymmetrical visual pathway. *Neuron* **93**, 914–928.e4 (2017).
24. K. J. Turner, T. A. Hawkins, J. Yáñez, R. Anadón, S. W. Wilson, M. Folgueira, Afferent connectivity of the zebrafish habenulae. *Front. Neural Circuits* **10**, 30 (2016).
25. M. Matsumoto, O. Hikosaka, Lateral habenula as a source of negative reward signals in dopamine neurons. *Nature* **447**, 1111–1115 (2007).
26. I. Lazaridis, O. Tzortzi, M. Weglage, A. Märtin, Y. Xuan, M. Parent, Y. Johansson, J. Fuzik, D. Fürth, L. E. Fenno, C. Ramakrishnan, G. Silberberg, K. Deisseroth, M. Carlén, K. Meletis, A hypothalamus-habenula circuit controls aversion. *Mol. Psychiatry* **24**, 1351–1368 (2019).
27. E. R. Duboué, E. Hong, K. C. Eldred, M. E. Halpern, Left habenular activity attenuates fear responses in larval zebrafish. *Curr. Biol.* **27**, 2154–2162.e3 (2017).
28. Y. Yang, Y. Cui, K. Sang, Y. Dong, Z. Ni, S. Ma, H. Hu, Ketamine blocks bursting in the lateral habenula to rapidly relieve depression. *Nature* **554**, 317–322 (2018).
29. T. N. deCarvalho, A. Subedi, J. Rock, B. D. Harfe, C. Thisse, B. Thisse, M. E. Halpern, E. Hong, Neurotransmitter map of the asymmetric dorsal habenular nuclei of zebrafish. *Genesis* **52**, 636–655 (2014).
30. S. Pandey, K. Shekhar, A. Regev, A. F. Schier, Comprehensive identification and spatial mapping of habenular neuronal types using single-cell RNA-seq. *Curr. Biol.* **28**, 1052–1065.e7 (2018).
31. M. Agetsuma, H. Aizawa, T. Aoki, R. Nakayama, M. Takahoko, M. Goto, T. Sassa, R. Amo, T. Shiraki, K. Kawakami, T. Hosoya, S.-i. Higashijima, H. Okamoto, The habenula is crucial for experience-dependent modification of fear responses in zebrafish. *Nat. Neurosci.* **13**, 1354–1356 (2010).
32. R. Amo, H. Aizawa, M. Takahoko, M. Kobayashi, R. Takahashi, T. Aoki, H. Okamoto, Identification of the zebrafish ventral habenula as a homolog of the mammalian lateral habenula. *J. Neurosci.* **30**, 1566–1574 (2010).
33. R. Amo, F. Fredes, M. Kinoshita, R. Aoki, H. Aizawa, M. Agetsuma, T. Aoki, T. Shiraki, H. Kakinuma, M. Matsuda, M. Yamazaki, M. Takahoko, T. Tsuboi, S.-i. Higashijima, N. Miyasaka, T. Koide, Y. Yabuki, Y. Yoshihara, T. Fukai, H. Okamoto, The habenulo-raphe serotonergic circuit encodes an aversive expectation value essential for adaptive active avoidance of danger. *Neuron* **84**, 1034–1048 (2014).
34. E. Dreosti, N. V. Llopis, M. Carl, E. Yaksi, S. W. Wilson, Left-right asymmetry is required for the habenulae to respond to both visual and olfactory stimuli. *Curr. Biol.* **24**, 440–445 (2014).
35. S. K. Jetti, N. Vendrell-Llopis, E. Yaksi, Spontaneous activity governs olfactory representations in spatially organized habenular microcircuits. *Curr. Biol.* **24**, 434–439 (2014).
36. M.-Y. Chou, R. Amo, M. Kinoshita, B.-W. Cherng, H. Shimazaki, M. Agetsuma, T. Shiraki, T. Aoki, M. Takahoko, M. Yamazaki, S.-i. Higashijima, H. Okamoto, Social conflict resolution regulated by two dorsal habenular subregions in zebrafish. *Science* **352**, 87–90 (2016).
37. A. S. Andalman, V. M. Burns, M. Lovett-Barron, M. Broxton, B. Poole, S. J. Yang, L. Grosenick, T. N. Lerner, R. Chen, T. Benster, P. Mourrain, M. Levoy, K. Rajan, K. Deisseroth, Neuronal dynamics regulating brain and behavioral state transitions. *Cell* **177**, 970–985.e20 (2019).
38. H. Aizawa, M. Goto, T. Sato, H. Okamoto, Temporally regulated asymmetric neurogenesis causes left-right difference in the zebrafish habenular structures. *Dev. Cell* **12**, 87–98 (2007).
39. I. H. Bianco, M. Carl, C. Russell, J. D. W. Clarke, S. W. Wilson, Brain asymmetry is encoded at the level of axon terminal morphology. *Neural Dev.* **3**, 9 (2008).
40. Y. Hashikawa, K. Hashikawa, M. A. Rossi, M. L. Basiri, Y. Liu, N. L. Johnston, O. R. Ahmad, G. D. Stuber, Transcriptional and spatial resolution of cell types in the mammalian habenula. *Neuron* **106**, 743–758.E5 (2020).
41. N. Vladimirov, Y. Mu, T. Kawashima, D. V. Bennett, C.-T. Yang, L. L. Looger, P. J. Keller, J. Freeman, M. B. Ahrens, Light-sheet functional imaging in fictively behaving zebrafish. *Nat. Methods* **11**, 883–884 (2014).
42. C. Satou, Y. Kimura, H. Hirata, M. L. Suster, K. Kawakami, S.-i. Higashijima, Transgenic tools to characterize neuronal properties of discrete populations of zebrafish neurons. *Development* **140**, 3927–3931 (2013).
43. S. Krishnan, A. S. Mathuru, C. Kibat, M. Rahman, C. E. Lupton, J. Stewart, A. Claridge-Chang, S.-C. Yen, S. Jesuthasan, The right dorsal habenula limits attraction to an odor in zebrafish. *Curr. Biol.* **24**, 1167–1175 (2014).
44. E. K. Scott, H. Baier, The cellular architecture of the larval zebrafish tectum, as revealed by gal4 enhancer trap lines. *Front. Neural Circuits* **3**, 13 (2009).
45. T. Koide, N. Miyasaka, K. Morimoto, K. Asakawa, A. Urasaki, K. Kawakami, Y. Yoshihara, Olfactory neural circuitry for attraction to amino acids revealed by transposon-mediated gene trap approach in zebrafish. *Proc. Natl. Acad. Sci. U.S.A.* **106**, 9884–9889 (2009).
46. F. Kermen, L. Darnet, C. Wiest, F. Palumbo, J. Bechert, O. Uslu, E. Yaksi, Stimulus-specific behavioral responses of zebrafish to a large range of odors exhibit individual variability. *BMC Biol.* **18**, 66 (2020).
47. A. S. Mathuru, C. Kibat, W. F. Cheong, G. Shui, M. R. Wenk, R. W. Friedrich, S. Jesuthasan, Chondroitin fragments are odorants that trigger fear behavior in fish. *Curr. Biol.* **22**, 538–544 (2012).
48. H. A. Burgess, M. Granato, Sensorimotor gating in larval zebrafish. *J. Neurosci.* **27**, 4984–4994 (2007).
49. E. Yaksi, B. Judkewitz, R. W. Friedrich, Topological reorganization of odor representations in the olfactory bulb. *PLOS Biol.* **5**, e178 (2007).
50. G. Buzsaki, A. Draguhn, Neuronal oscillations in cortical networks. *Science* **304**, 1926–1929 (2004).
51. S. A. Romano, V. Pérez-Schuster, A. Jouary, J. Boulanger-Weill, A. Candeo, T. Pietri, G. Sumbre, An integrated calcium imaging processing toolbox for the analysis of neuronal population dynamics. *PLOS Comput. Biol.* **13**, e1005526 (2017).
52. O. Randlett, C. L. Wee, E. A. Naumann, O. Nnaemeka, D. Schoppik, J. E. Fitzgerald, R. Portugues, A. M. B. Lacoste, C. Riegler, F. Engert, A. F. Schier, Whole-brain activity mapping onto a zebrafish brain atlas. *Nat. Methods* **12**, 1039–1046 (2015).
53. S.-Y. Yeo, M. J. Kim, H.-S. Kim, T.-L. Huh, A. B. Chitnis, Fluorescent protein expression driven by her4 regulatory elements reveals the spatiotemporal pattern of Notch signaling in the nervous system of zebrafish embryos. *Dev. Biol.* **301**, 555–567 (2007).
54. S. Govindan, P. Oberst, D. Jabaudon, In vivo pulse labeling of isochronic cohorts of cells in the central nervous system using FlashTag. *Nat. Protoc.* **13**, 2297–2311 (2018).

55. E. W. Olstad, C. Ringers, J. N. Hansen, A. Wens, C. Brandt, D. Wachten, E. Yaksi, N. Jurisch-Yaksi, Ciliary beating compartmentalizes cerebrospinal fluid flow in the brain and regulates ventricular development. *Curr. Biol.* **29**, 229–241.e6 (2019).
56. J. G. M. Bergboer, C. Wyatt, C. Austin-Tse, E. Yaksi, I. A. Drummond, Assaying sensory ciliopathies using calcium biosensor expression in zebrafish ciliated olfactory neurons. *Cilia* **7**, 2 (2018).
57. R.-K. Cheng, S. Krishnan, Q. Lin, C. Kibat, S. Jesuthasan, Characterization of a thalamic nucleus mediating habenula responses to changes in ambient illumination. *BMC Biol.* **15**, 104 (2017).
58. M. R. Warden, A. Selimbeyoglu, J. J. Mirzabekov, M. Lo, K. R. Thompson, S.-Y. Kim, A. Adhikari, K. M. Tye, L. M. Frank, K. Deisseroth, A prefrontal cortex-brainstem neuronal projection that controls response to behavioural challenge. *Nature* **492**, 428–432 (2012).
59. H.-p. Xu, M. Furman, Y. S. Mineur, H. Chen, S. L. King, D. Zenisek, Z. J. Zhou, D. A. Butts, N. Tian, M. R. Picciotto, M. C. Crair, An instructive role for patterned spontaneous retinal activity in mouse visual map development. *Neuron* **70**, 1115–1127 (2011).
60. Y. Cui, Y. Yang, Z. Ni, Y. Dong, G. Cai, A. Foncelle, S. Ma, K. Sang, S. Tang, Y. Li, Y. Shen, H. Berry, S. Wu, H. Hu, Astroglial Kir4.1 in the lateral habenula drives neuronal bursts in depression. *Nature* **554**, 323–327 (2018).
61. C. D. Verdugo, S. Myren-Svelstad, E. Aydin, E. Van Hoeymissen, C. Deneubourg, S. Vanderhaeghe, J. Vancraeynest, R. Pelgrims, M. I. Cosacak, A. Muto, C. Kizil, K. Kawakami, N. Jurisch-Yaksi, E. Yaksi, Glia-neuron interactions underlie state transitions to generalized seizures. *Nat. Commun.* **10**, 3830 (2019).
62. S. Hong, O. Hikosaka, The globus pallidus sends reward-related signals to the lateral habenula. *Neuron* **60**, 720–729 (2008).
63. P. Lal, H. Tanabe, M. L. Suster, D. Ailani, Y. Kotani, A. Muto, M. Itoh, M. Iwasaki, H. Wada, E. Yaksi, K. Kawakami, Identification of a neuronal population in the telencephalon essential for fear conditioning in zebrafish. *BMC Biol.* **16**, 45 (2018).
64. J. W. von Trotha, P. Vernier, L. Bally-Cuif, Emotions and motivated behavior converge on an amygdala-like structure in the zebrafish. *Eur. J. Neurosci.* **40**, 3302–3315 (2014).
65. G. Furlan, V. Cuccioli, N. Vuillemin, L. Dirian, A. J. Muntasell, M. Coolen, N. Dray, S. Bedu, C. Houart, E. Beaurepaire, I. Foucher, L. Bally-Cuif, Life-long neurogenic activity of individual neural stem cells and continuous growth establish an outside-in architecture in the teleost pallium. *Curr. Biol.* **27**, 3288–3301.e3 (2017).
66. N. Jurisch-Yaksi, E. Yaksi, C. Kizil, Radial glia in the zebrafish brain: Functional, structural, and physiological comparison with the mammalian glia. *Glia*, (2020).
67. M. B. Luskin, C. J. Shatz, Neurogenesis of the cat's primary visual cortex. *J. Comp. Neurol.* **242**, 611–631 (1985).
68. J. A. Lister, C. P. Robertson, T. Lepage, S. L. Johnson, D. W. Raible, Nacre encodes a zebrafish microphthalmia-related protein that regulates neural-crest-derived pigment cell fate. *Development* **126**, 3757–3767 (1999).
69. H.-C. Park, C.-H. Kim, Y.-K. Bae, S.-Y. Yeo, S.-H. Kim, S.-K. Hong, J. Shin, K.-W. Yoo, M. Hibi, T. Hirano, N. Miki, A. BChitnis, T.-L. Huh, Analysis of upstream elements in the HuC promoter leads to the establishment of transgenic zebrafish with fluorescent neurons. *Dev. Biol.* **227**, 279–293 (2000).
70. F. Kermen, P. Lal, N. G. Faturos, E. Yaksi, Interhemispheric connections between olfactory bulbs improve odor detection. *PLoS Biol.* **18**, e3000701 (2020).
71. I. Reiten, F. E. Uslu, S. Fore, R. Pelgrims, C. Ringers, C. D. Verdugo, M. Hoffman, P. Lal, K. Kawakami, K. Pekkan, E. Yaksi, N. Jurisch-Yaksi, Motile-cilia-mediated flow improves sensitivity and temporal resolution of olfactory computations. *Curr. Biol.* **27**, 166–174 (2017).
72. Bergen, J. R., Anandan, P., Hanna, K. J., Hingorani, R. Hierarchical model-based motion estimation, in *ECCV '92; Proceedings of the Second European Conference on Computer Vision* (Springer Berlin Heidelberg, 1992), pp. 237–252.

Acknowledgments: We thank M. Ahrens (HHMI, Janelia Farm, USA), C. Wyart (ICM, Paris, France), H. Baier (MPI, Martinsried, Germany), and S.-i. Higashijima (Okazaki Institute for Integrative Bioscience, Japan) for transgenic lines. We thank S. Eggen, M. Andresen, V. Nguyen, and our fish facility support team for technical assistance. We thank the Yaksi laboratory members for stimulating discussions. **Funding:** This work was funded by ERC starting grant 335561 (S.F. and E.Y.), Helse Midt-Norge Samarbeidsorganet grant (N.J.-Y. and E.Y.), RCN FRIPRO Research Grant 239973 (E.Y.), and Boehringer Ingelheim Fonds (C.R.). Work in the E.Y. laboratory is funded by the Kavli Institute for Systems Neuroscience at NTNU. **Ethics statement:** All experimental procedures performed on zebrafish larvae and juveniles were in accordance with the Directive 2010/63/EU of the European Parliament and the Council of the European Union and approved by the Norwegian Food Safety Authorities and Landesdirektion Sachsen, Germany (permit numbers TVV-52/2015 and TVV-35/2016). **Author contributions:** Conceptualization: S.F. and E.Y. Methodology and data: S.F., F.A-H., K.A.M., E.M.B., B.S., N.G.F., K.T.P.C., M.I.C., N.J.-Y., and C.K. Data analysis: S.F., F.A-H., K.A.M., E.M.B., B.S., N.G.F., K.T.P.C., C.D.V., F.P., C.R., and N.J.-Y. Investigation: all authors. Writing: S.F., F.A-H., and E.Y. Review and editing: all authors. Funding acquisition and supervision: E.Y. **Competing interests:** The authors declare that they have no competing interests. **Data and materials availability:** All data needed to evaluate the conclusions in the paper are present in the paper and/or the Supplementary Materials. Additional data related to this paper may be requested from the authors.

Submitted 29 August 2019
Accepted 17 July 2020
Published 4 September 2020
10.1126/sciadv.aaz3173

Citation: S. Fore, F. Acuña-Hinrichsen, K. A. Mutlu, E. M. Bartoszek, B. Serneels, N. G. Faturos, K. T. P. Chau, M. I. Cosacak, C. D. Verdugo, F. Palumbo, C. Ringers, N. Jurisch-Yaksi, C. Kizil, E. Yaksi, Functional properties of habenular neurons are determined by developmental stage and sequential neurogenesis. *Sci. Adv.* **6**, eaaz3173 (2020).